iScience

CellPress
OPEN ACCESS

Article

The mouse epididymal amyloid matrix is a mammalian counterpart of a bacterial biofilm

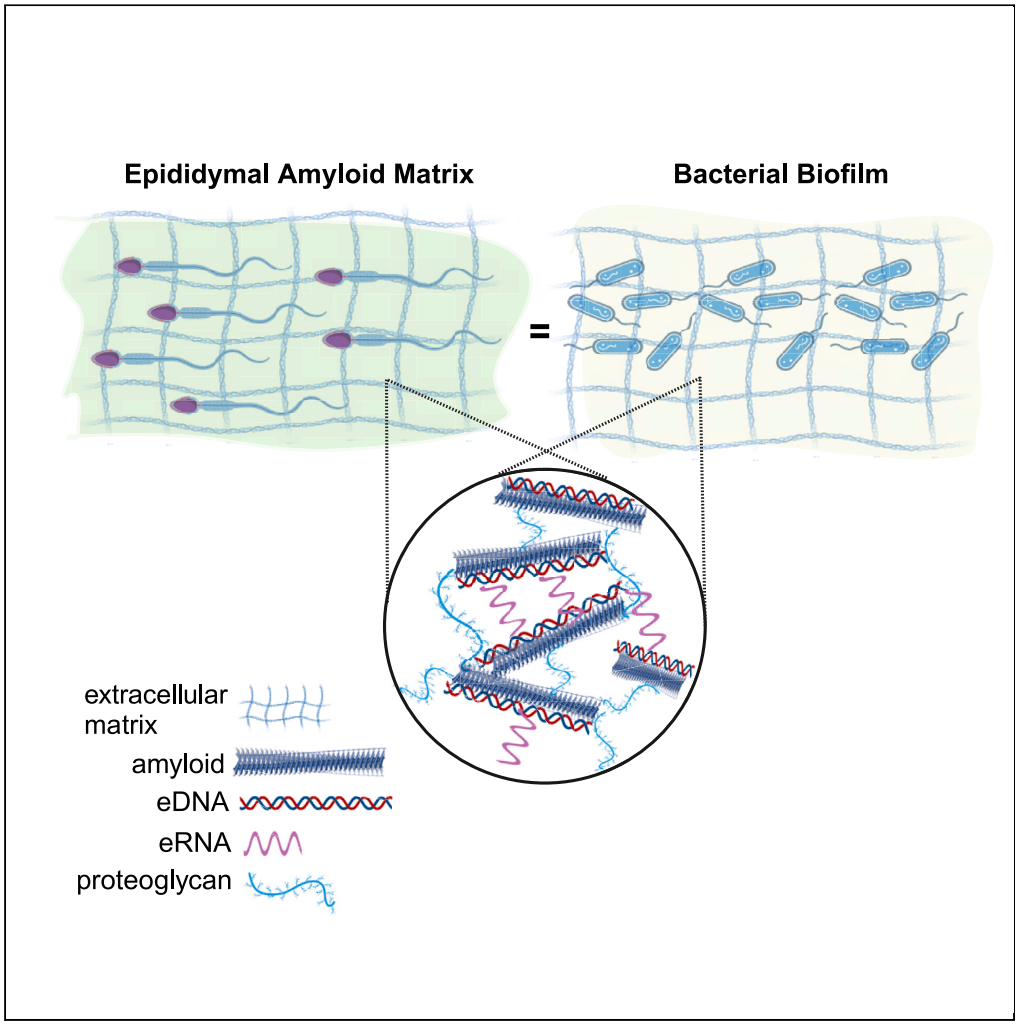

Caitlyn Myers, Georgia Rae Atkins, Johanna Villarreal, R. Bryan Sutton, Gail A. Cornwall

gail.cornwall@ttuhsc.edu

Highlights

The mouse epididymal amyloid matrix resembles a bacterial biofilm

The epididymal amyloid matrix contains amyloid, eDNA/eRNA, and polysaccharides

Epididymal amyloid matrix components have functions comparable to those in biofilms

The building blocks of specialized ECM are evolutionarily conserved

Myers et al., iScience 27, 110152
June 21, 2024
https://doi.org/10.1016/j.isci.2024.110152

iScience

CellPress
OPEN ACCESS

Article

The mouse epididymal amyloid matrix is a mammalian counterpart of a bacterial biofilm

Caitlyn Myers,[1,3] Georgia Rae Atkins,[1,4] Johanna Villarreal,[2] R. Bryan Sutton,[2] and Gail A. Cornwall[1,5,*]

SUMMARY

The mouse epididymis is a long tubule connecting the testis to the vas deferens. Its primary functions are to mature spermatozoa into motile and fertile cells and to protect them from pathogens that ascend the male tract. We previously demonstrated that a functional extracellular amyloid matrix surrounds spermatozoa in the epididymal lumen and has host defense functions, properties not unlike that of an extracellular biofilm that encloses and protects a bacterial community. Here we show the epididymal amyloid matrix also structurally resembles a biofilm by containing eDNA, eRNA, and mucin-like polysaccharides. Further these structural components exhibit comparable behaviors and perform functions such as their counterparts in bacterial biofilms. Our studies suggest that nature has used the ancient building blocks of bacterial biofilms to form an analogous structure that nurtures and protects the mammalian male germline.

INTRODUCTION

The epididymis is a highly convoluted tubule connecting the testis to the vas deferens. Its primary functions are to mature spermatozoa into motile and fertile cells and to protect them from pathogens that ascend the male tract. Because spermatogenesis occurs after self-tolerance is established, spermatozoa are naturally antigenic.[1,2] Therefore, the epididymal lumen is an immunologically unique compartment. It maintains a tolerant environment for spermatozoa to enable their maturation into functional cells while at the same time can mount a host defense response against pathogens. Precisely how the epididymis carries out and coordinates these two critical functions remains unclear.

We previously showed that the mouse epididymis contains a functional extracellular amyloid matrix that fills the lumen and contains the maturing spermatozoa.[3] The epididymal amyloid matrix includes cystatin C and several CRES (cystatin-related epididymal spermatogenic) subgroup family members including CRES, CRES2, CRES3, and cystatin E2.[4] Unlike cystatin C, CRES subgroup members lack consensus sites for cysteine protease inhibition suggesting unique biological roles.[5] Indeed, CRES, CRES2, CRES3, and cystatin E2 are highly aggregation-prone, each forming amyloids with distinct assembly properties *in vitro*.[4] Further, CRES3 and CRES can cross-seed suggesting interactions between subgroup members, possibly by the formation of heterooligomers, may regulate epididymal amyloid matrix assembly.[6] We recently demonstrated that CRES amyloids and the epididymal amyloid matrix have host defense functions and adopt different amyloid structures (matrix, film, fibrils) with different antimicrobial functions (bacterial trapping, killing, promotion of ghost-like bacteria) depending on the pathogenicity of the bacterial strain.[7] Thus, the shape-shifting properties of the amyloid matrix allow for a plasticity that is integral for its functions.

The contribution of several amyloidogenic CRES subgroup members to the assembly of a mammalian host defense structure is strikingly like the amyloidogenic curli family of proteins that organize the assembly of *E. coli* biofilms.[8] Curli member B (CsgB) serves as a nucleator to initiate curli A (CsgA) amyloid assembly at the bacterial cell surface forming the infrastructure of the extracellular biofilm.[9] A primary function of biofilms is to nurture the bacteria within them by providing a safe environment which is stable and rich in nutrients.[10] Biofilms also protect bacteria from antibiotics, pathogens, and other harmful factors making them especially efficient host defense structures.[11] Based on these structural and functional similarities, we hypothesized the epididymal amyloid matrix may be a mammalian counterpart of a bacterial biofilm. However, rather than nurturing and protecting a bacterial colony as a biofilm would do, the epididymal amyloid matrix nurtures/matures and protects the male germline.

The structural components of bacterial biofilms have long been studied as potential therapeutic targets for dispersing bacteria during infections.[12] Biofilms are composed of bacteria and extracellular polymeric substances (EPS) that can include amyloid, extracellular DNA (eDNA), extracellular RNA (eRNA), and polysaccharides.[13] The many roles these components perform in the formation and function of biofilms are still an area of intense study. Amyloids serve an essential function as a structural scaffold interacting with other extracellular components in the biofilm.[14] They also can contribute to the adherence of the biofilm to substrates and perform a protective role by trapping phage

[1]Department of Cell Biology and Biochemistry, Texas Tech University Health Sciences Center, Lubbock, TX 79430, USA
[2]Department of Cell Physiology and Molecular Biophysics, Texas Tech University Health Sciences Center, Lubbock, TX 79430, USA
[3]Present address: Department of Microbiology and Immunology, Institute of Biomedicine, University of Gothenburg, Gothenburg, Sweden
[4]Present address: Department of Obstetrics, Gynecology and Reproductive Sciences, University of Pittsburgh School of Medicine, Pittsburgh, PA, USA
[5]Lead contact
*Correspondence: gail.cornwall@ttuhsc.edu
https://doi.org/10.1016/j.isci.2024.110152

particles.[15,16] eDNA can have several roles in biofilms, including in its formation by templating amyloid assembly,[17] regulation of its maturation,[18] maintenance of overall structure,[19–21] cell adhesion,[22] horizontal gene transfer,[23] and protection from antibiotics.[24] More recently, eRNA has also been shown to be a component of some biofilms, and such as eDNA, contributes to overall biofilm structure including its distinctive viscoelastic properties.[25] Further, several noncoding RNAs have been shown to regulate biofilm assembly by mediating curli production and exopolysaccharide synthesis.[26] Polysaccharides, often mucopolysaccharides/glycosaminoglycans, are the major component of the EPS providing the "glue" important for the structure and adhesive properties of the biofilm. These long linear chains of sugars also stratify the bacteria within the community[27,28] and form a physical barrier or protective coat that can promote a tolerogenic immune response for bacteria.[27,29–31] Their ability to protect eDNA/eRNA from degradation by nucleases suggests a close association between polysaccharides and nucleic acids within the biofilm.[32] Similar to eDNA, polysaccharides including sulfated forms have been shown to template amyloid assembly.[33,34]

Here, we carried out studies to characterize the structural components of the mouse epididymal amyloid matrix to determine if it has the properties of a bacterial biofilm and contains extracellular DNA, RNA, and polysaccharides. Further, we determined if these structures perform similar functions and exhibit comparable behaviors as their counterparts in bacterial biofilms. Establishing the component parts of the epididymal amyloid matrix is key for elucidating the mechanisms of its assembly, host defense functions, and interactions with its resident cells, the spermatozoa. This knowledge is essential for developing much needed therapies for male infertility including that as a result of luminal occlusions formed following bacterial infections.[35] Discovering parallels between the epididymal amyloid matrix and biofilm structures/functions also could prove insightful for identifying basic mechanisms essential for cell/species survival, including those mediated by environmentally driven epigenetic modifications. We demonstrate that eRNA, eDNA, and mucin-like polysaccharides are key components of the epididymal amyloid matrix and play critical roles in maintaining its overall structure. Together, our studies reveal how nature has preserved the ancient building blocks of biofilms to construct a structure that nurtures/protects the mammalian male germline.

RESULTS

Extracellular DNA and extracellular RNA are components of the epididymal amyloid matrix

We used differential centrifugation to isolate fractions containing distinct populations of the epididymal amyloid matrix (pellets 2 and 4 (P2, P4)) from the mouse caput and corpus-cauda (from here on referred to as cauda) epididymis (Figures 1A and 1B). Because the corpus is the thinnest part of the epididymis and lacked sufficient material for our analyses, it was combined with the cauda region. Our previous studies suggest the amyloid matrix is assembling in the most proximal part of the epididymis (caput) as sperm enter from the testis, forming a highly branched matrix that transitions into fibrillar arrays in the distal/cauda epididymis.[7] The P2 and P4 fractions may represent precursor (early condensates) and more mature amyloid assemblies (matrix, fibrils), respectively, within each region. We did not examine the P3 pellet since there was very little material in this fraction, especially from the cauda region. The P2 and P4 amyloid-containing fractions were spread on a slide and stained with Sytox Green, Hoechst, and TOTO-3, fluorescent dyes commonly used to visualize nucleic acids, and thioflavin S (ThS), a fluorescent dye that recognizes the cross-β sheet structure of amyloid. Although the nucleic acid dyes are routinely used as indicators of DNA, they also can bind RNA. As shown in Figures 1C and 1D both the P2 and P4 fractions from the caput epididymis and P4 fraction from the cauda epididymis were stained with the nucleic acid dyes and ThS indicating the presence of nucleic acids within the amyloid matrix. Specifically, in the caput P2 fraction nucleic acid fluorescence was primarily observed in small particles distributed throughout a granular layer (Figure 1C) while in the caput P4 fraction nucleic acid staining was present in larger particles and as part of film-like structures. In contrast to the caput fractions, nucleic acid fluorescence in the cauda P4 fraction was diffuse and decreased in intensity (Figure 1D). Pretreatment of the caput P2 and P4 amyloids with 5% SDS, which helped expose the amyloid as indicated by increased ThS fluorescence and by an overall change in amyloid matrix appearance, caused the nucleic acid fluorescence to become less punctate and more dispersed, which was especially noticeable with TOTO-3 staining in the caput P4 fraction. Exposure of the cauda P4 amyloid to 70% formic acid also resulted in a slight increase in ThS fluorescence, however, less of an effect was observed on the intensity or pattern of nucleic acid staining (Figure 1D). Formic acid instead of SDS was needed to facilitate exposure of the amyloid in the cauda P4 fraction consistent with it being a more mature structure in this region.

We next performed experiments in which the caput and cauda amyloid samples were costained with ThS and propidium idodide, also a nucleic acid stain. The merged fluorescent images show that nucleic acid is present within ThS positive material suggesting it is part of the amyloid matrix (Figure 2). Although the merged images suggest a complete co-localization of nucleic acids and amyloid, minor bleed through of the ThS signal to the red channel was sometimes observed and therefore further high resolution/deconvolution imaging studies are needed to specifically determine where nucleic acids reside within the three-dimensional epididymal amyloid matrix.

To confirm the presence of nucleic acids and to determine the size associated with the P2 and P4 amyloids, we analyzed the samples by agarose gel electrophoresis and ethidium bromide (EtBr) staining. Caput P2 amyloid contained several populations of nucleic acids; that which was of high molecular mass and did not enter very far into the gel (red arrow), those of intermediate size approximately 1.5–5 kb, and a population at 250 bp (Figure 3A). High, intermediate (although slightly larger than those in P2) and low molecular mass nucleic acid populations were also detected in the caput P4 amyloid but overall, there was less EtBr staining compared to caput P2. Because P4 may be a more highly ordered amyloid than P2 it may not completely enter the gel or unwind sufficiently to allow robust EtBr staining. Caput luminal fluid that did not undergo centrifugation (total) also showed nucleic acid forms like those in the caput P2 and P4 amyloids (Figure 3A). The supernatant fraction (S) obtained from the final centrifugation step to generate the P4 pellet did not exhibit any EtBr staining showing

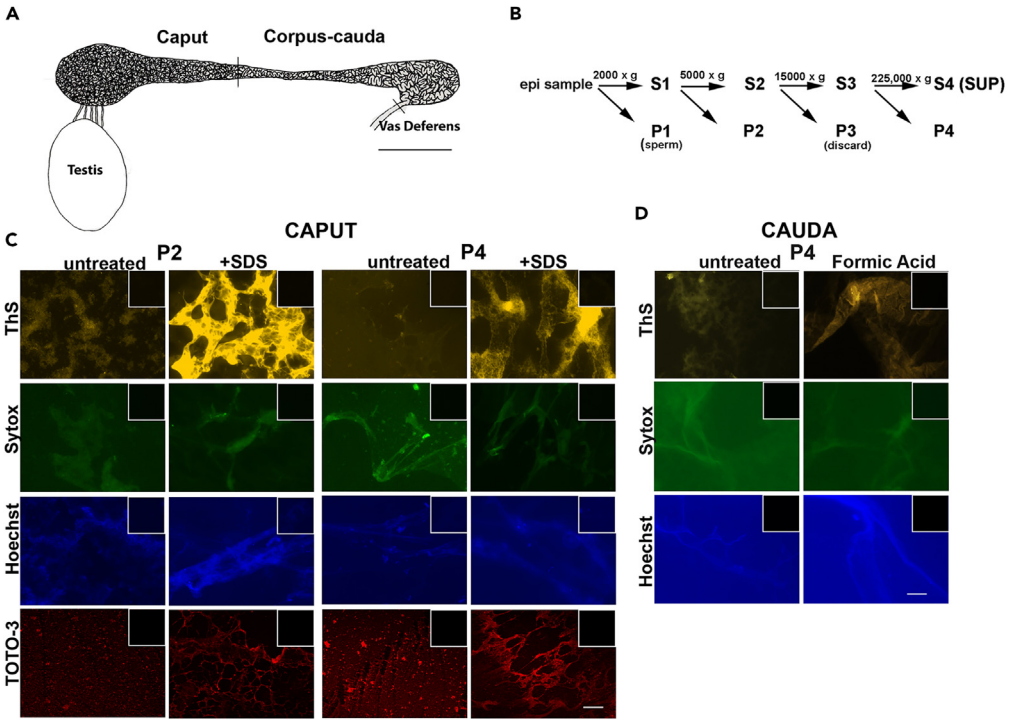

Figure 1. Extracellular nucleic acids are present in the epididymal amyloid matrix

(A) Schematic diagram of the rodent epididymis showing the caput and corpus-cauda (cauda) regions and its connections to the testis and vas deferens. Scale bar, 3 mm.

(B) Differential centrifugation protocol used to isolate fractions enriched in amyloids of different molecular mass from the caput and cauda epididymal lumen. S, supernatant; P, pellet. The P3 pellet contained little material and was not studied further.

Isolated amyloid matrix from C) caput P2 and P4 and D) cauda P4 were stained with the amyloid dye, Thioflavin S (ThS) or nucleic acid stains, Sytox Green, Hoechst, and TOTO-3 and imaged using a Zeiss Axiovert 200M microscope equipped with epifluorescence. Caput P2 and P4 were also treated with 5% SDS while cauda P4 was treated with 70% formic acid for 15 min at room temperature to facilitate unwinding of the structure before staining. Insets, control, mock-stained samples in the absence of ThS or nucleic acid stains. Scale bar, 20 μm.

nucleic acids are only present in the particulate fraction. In the cauda epididymis the predominant populations of nucleic acid in the P2, P4 and total amyloid fractions were that which were of high molecular mass and a population at 250 bp (Figure 3A).

To determine if the EtBr staining in the epididymal amyloids represented eDNA, we incubated caput and cauda P4 amyloids with DNases and then determined the degree of degradation by agarose gel electrophoresis. DNase1 and DNase1L3 (DNase 1 like 3) are both Ca^{2+}/Mg^{2+} - dependent endonucleases that participate in clearance of serum eDNA; however, DNase1L3 uniquely degrades antigenic forms of cell-free DNA, including DNA complexed with lipids and proteins.[36] We used a plasmid degradation assay to compare the activity of DNase1L3 prepared in-house to that of a commercially purchased DNase1. Approximately 50% of plasmid DNA was digested by 0.5 μg/mL DNase1 while a similar percentage of plasmid digestion required 2 μg/mL of DNase1L3 (Figure S1, arrows) suggesting the DNases have different activities or specificities. We then compared these two concentrations of DNase1 and DNase1L3 in their ability to digest the caput and cauda P4 amyloid matrix (Figure 3B). In addition, we compared the activity of both DNases at 5 μg/mL, a concentration at which the plasmid was completely digested by the two enzymes. Compared to control samples incubated in buffer, after 1 h at 37°C DNase1L3 (2 μg/mL and 5 μg/mL) reduced the levels of the high molecular mass and 1.5–5 kb nucleic acid forms in the caput P4 amyloid but had no effect on the small 250 bp population (Figure 3B, left panel). Similarly, DNase1L3 digested some, but not all, of the high molecular mass nucleic acids in the cauda P4 amyloid (Figure 3B, right panel). In contrast, there was no digestion of nucleic acids in the cauda P4 amyloids after incubation with DNase1, and only a slight digestion of the caput P4 amyloid at its highest concentration of 5 μg/mL (Figure 3B, left panel). Together these results suggest eDNA is a component of the epididymal amyloid matrix and is present in several distinct populations including that which is resistant to, or protected from, DNase. The preferential ability of DNase1L3 to digest eDNA in the P4 amyloid over that of DNase1 is consistent with its known ability to degrade DNA complexed to protein.[37]

We next determined if eRNA was present in the epididymal P4 amyloid. DNase-free RNase completely digested all the populations of nucleic acid in the caput epididymal P4 amyloid matrix except for the high molecular mass population (Figure 3C, red arrow). Together our results suggest the intermediate and small sized nucleic acids in the epididymal amyloids are RNA while the high molecular mass population is DNA. The slight digestion of the 1.5–5 kb population of nucleic acids by DNase1L3 suggests the enzyme may also possess some RNase activity in addition to its primary DNase functions (Figure 3B). Because the P4 amyloid preparations likely also contain extracellular

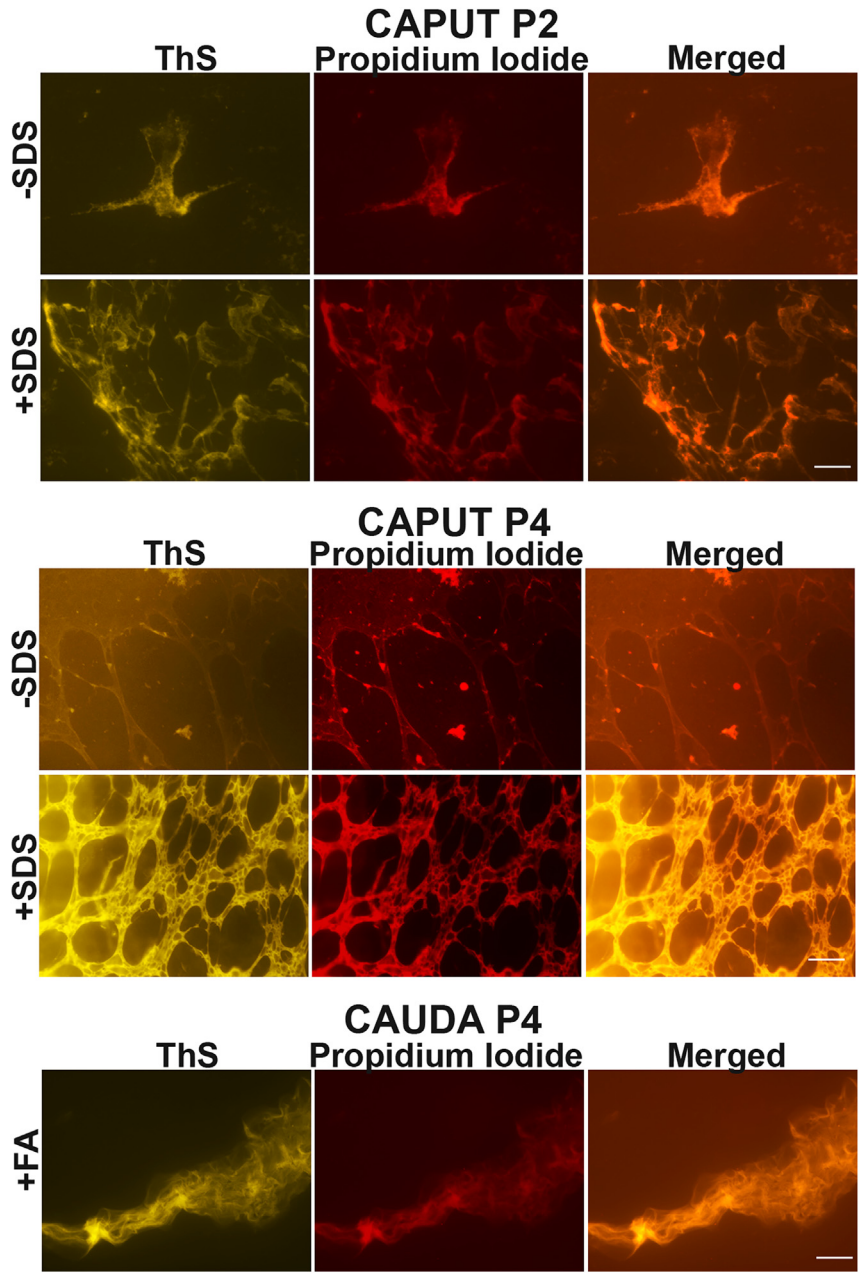

Figure 2. Extracellular nucleic acids are present with amyloid in the epididymal amyloid matrix

Caput P2, caput, and cauda P4 amyloids were stained with ThS to detect amyloid followed by propidium iodide to detect nucleic acid. Some caput P4 samples were treated with 5% SDS for 15 min while some cauda P4 samples were treated with 70% formic acid (FA) for 15 min prior to staining with ThS and propidium iodide. Scale bar, 20 μm.

vesicles/exosomes with DNA/RNA cargo we cannot rule out that some EtBr staining reflects these other populations of nucleic acids. It is also possible that some intracellular nucleic acids were released from the epididymal epithelial cells during the isolation of the amyloid fractions.

Extracellular DNA and RNA are necessary for the maintenance of the epididymal amyloid matrix structure

Experiments were next carried out to determine if a function of eDNA is to maintain epididymal amyloid matrix structure. Caput P2 and caput and cauda P4 amyloids were incubated with 5 μg/mL DNase1L3 and stained with the nucleic acid stain Sytox Orange and ThS to determine if DNA digestion resulted in a change in the amyloid matrix structure. In this experiment, cauda P4 was not pretreated with formic acid to unwind/expose the amyloid and therefore, compared to the caput, longer exposure times were needed during imaging of ThS and Sytox

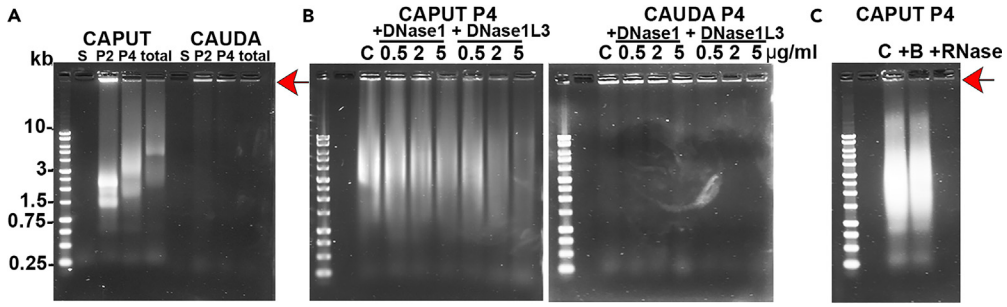

Figure 3. The epididymal amyloid matrix contains distinct populations of eDNA and eRNA

(A) Twenty µgs of supernatant (S4/S), P2, P4 amyloid fractions and total luminal fluid (total) isolated from caput and cauda epididymis were separated on a 1% agarose-TAE gel and stained with EtBr to visualize nucleic acid. Red arrow indicates high molecular mass population of nucleic acid.

(B) Twenty µgs of caput P4 (left panel) and cauda P4 (right panel) amyloid fractions were incubated with 0.5, 2.5 and 5 µm/mL DNase1 or DNase1L3 and analyzed by agarose gel electrophoresis and EtBr staining. C, control, P4 amyloid incubated in the absence of DNase.

(C) Twenty µgs of caput P4 amyloid were incubated with B, buffer or DNase-free RNase for 30 min followed by agarose gel electrophoresis and EtBr staining. Red arrow indicates the high molecular mass population of DNA. See also Figure S1.

Orange to visualize the effects of DNase. For this reason, direct comparisons in ThS and Sytox Orange fluorescence intensities cannot be made between the different populations of amyloids from the different epididymal regions.

Caput P2 and caput and cauda P4 starting samples (ST, amyloid fractions in dPBS or HEPES isolation buffer) contained their characteristic sheets of ThS positive film (granular in P2) (Figures 4, 5, and 6). Surprisingly, the addition of DNase reaction buffer alone affected the structure of the caput P2 and caput P4 amyloids. Specifically, the caput P2 amyloid starting sample, which typically exhibited a layer of small ThS positive granules, developed large holes/clear zones suggesting points of perturbation and a local unwinding of structure (Figure 4A). An overall loss of amyloid was indicated by a significant decrease ($p < 0.05$) in total ThT levels, as determined by plate assay of the P2 sample exposed to DNase buffer compared to the starting sample (Figure 4B). Nucleic acids, as indicated by Sytox Orange fluorescence, also had a speckled pattern in the starting caput P2 sample (Figure 4A) and were reduced after exposure to buffer except around the periphery of large holes where a thin edge of fluorescence (usually as a ring of speckles) was observed (Figure S2). Although rare, nucleic acids were sometimes observed in the clear zone itself. Because of this variable staining we were unable to measure a significant decrease in total nucleic acid levels in the P2 sample exposed to DNase reaction buffer compared to the starting sample (Figure 4C). Similarly, the caput P4 ThS positive amyloid film developed large holes, became fragmented, and exhibited reduced ($p < 0.05$) amyloid levels after exposure to the DNase buffer (Figures 5A and 5B). Caput P4 also exhibited reduced nucleic acid levels when visualized by fluorescence microscopy except around the edges of the large holes where Sytox Orange fluorescent speckles were observed (Figures 5A and S2). DNase buffer had little effect on the cauda P4 amyloid; while the ThS stained amyloid appeared more web-like, these changes were typically only noticeable on the edges of the amyloid layer (Figure 6A) and therefore significant changes in total amyloid and nucleic acid levels were not observed (Figures 6B and 6C). Further, unlike the caput P2 and P4 amyloids, large holes with bright Sytox Orange fluorescent edges were rarely seen in the cauda P4 amyloid after exposure to DNase buffer.

The only difference between the starting P2 and P4 amyloid samples and those incubated with DNase buffer was the presence of 1 mM $MgCl_2$. The addition of DNase buffer ($MgCl_2$) did not change overall protein content as indicated by Coomassie staining of P2 and P4 amyloid fractions before (ST, start) and after exposure (+B, buffer) (Figure S3). It is possible that Mg activated endogenous nucleases present in the epididymal lumen resulting in the formation of the clear zones.[38,39] Indeed, the addition of EDTA resulted in P2 and caput P4 amyloids that maintained their levels of amyloid and nucleic acids and exhibited structures comparable to that in the starting samples suggesting an inhibition of a Mg-dependent endogenous nuclease activity (Figures 4 and 5). However, we cannot rule out that Mg could also activate specific proteases that directly affected the amyloid matrix. Because of the effect of the buffer on the P2 and P4 amyloid and nucleic acid levels, we were unable to detect any additional changes in structure and in total amyloid and nucleic acid content after the addition of exogenous DNase1L3, even after a longer incubation time of 4 h (Figures 4, 5, and 6). The ring of Sytox Orange fluorescence around the buffer-induced holes remained, and even sometime appeared brighter (Figure S2). These results suggest that the exogenous DNase1L3 might help expose other populations of nucleic acids at sites where the amyloids have unwound/disassembled but whether these populations represent eRNA or DNase-resistant eDNA is not known.

Although the caput P2 and P4 amyloid films formed holes and fragments in the presence of DNase buffer (with and without DNase1L3) the amyloid matrix did not completely disassemble. These experiments further support that there may be several populations of eDNA associated with the amyloid matrix including those that are highly stable/resistant or inaccessible to DNase. Our results are consistent with those observed with the agarose gels showing high molecular mass DNA that remained following exposure to DNase1L3 (Figure 3). Although RNAsin was included during the incubations to prevent the effects of possible confounding RNases on amyloid matrix dispersion, whether RNAsin would be a functional inhibitor of a potential RNase activity from DNase1L3 is not known. Another possible reason why the epididymal amyloid did not completely disassemble is that other structural components, in addition to eDNA, contribute to the integrity of the epididymal amyloid matrix.

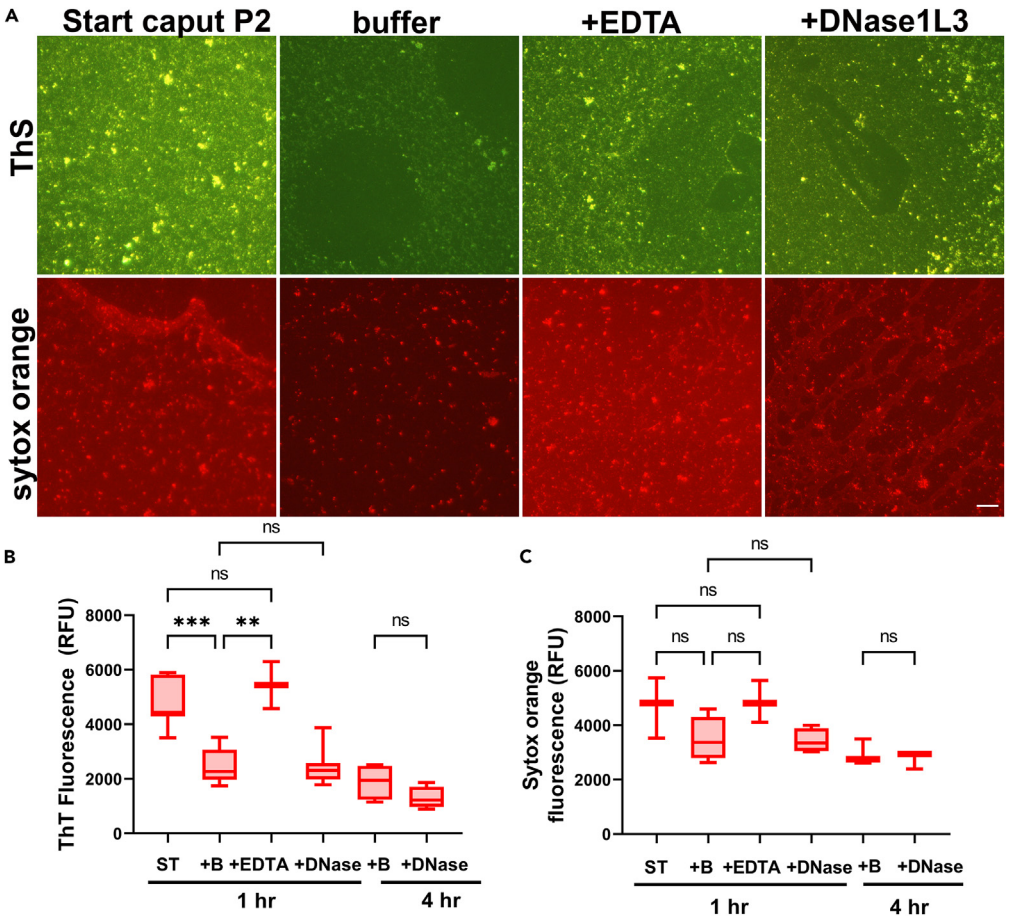

Figure 4. An endogenous activity partially disassembles the caput P2 epididymal amyloid matrix

(A) Caput P2 amyloid fractions (30 μgs) were incubated with DNase buffer (buffer, +B), DNase buffer + EDTA (+EDTA), or 5 μg/mL DNase1L3 (+DNAse1L3) for 1 h at 37°C. Start sample (ST) was caput P2 amyloid incubated in buffer without $MgCl_2$. Samples were dried overnight on a slide and incubated with ThS to visualize amyloid while a second set of samples were incubated with Sytox Orange to detect nucleic acids. Images were captured using a Zeiss Axiovert 200M microscope equipped with epifluorescence. Scale bar, 20 μm. See also Figure S2.

A proportion of each sample analyzed in A) was added to a 96 well plate in the presence of either B) 20 μM ThT or C) 0.2 μM Sytox Orange and relative fluorescence units measured with a Tecan plate reader. Caput P2 samples were also incubated for 4 h in DNase buffer only (+B) or DNase1L3 (+DNase). Data are represented as mean ± SEM from n = 3–8 experiments where each experiment used freshly isolated epididymal amyloid matrix. Statistical analyses were performed using ANOVA followed by multiple comparisons test in GraphPad Prism 9.5. *p = 0.01, **p = 0.002. n.s., not significant. See also Figure S3.

Therefore, we next carried out experiments to determine if eRNA also has a functional role in maintaining the epididymal amyloid matrix structure. The addition of DNase-free RNase caused the caput P2 and P4 amyloid to become fragmented as indicated by patchy ThS staining, with notably reduced ($p < 0.05$) amyloid and nucleic acid content (Figures 7A–7C). No exogenous $MgCl_2$ was included during the reactions and therefore samples exposed to buffer only served as controls since in these samples ThS, ThT, and Sytox Orange fluorescence were not different from that of starting P2 and P4 amyloids (data not shown). Although the effects of RNase on the structure of the cauda P4 amyloid were less pronounced than in the caput, some areas of the dense cauda P4 amyloid developed a swiss cheese appearance with small holes scattered throughout. However, while there was a loss of nucleic acids in the cauda P4 amyloid following RNase treatment, overall amyloid levels were not reduced (Figures 7A–7C). Because RNase exposure resulted in significant changes in nucleic acid content in all epididymal amyloid samples (Figure 7) ($p < 0.05$) suggests that eRNA within the epididymal amyloid matrix may be more accessible to nucleases than eDNA.

Epithelial cells are a source of nucleic acids in the epididymal amyloid matrix

There could be several possible sources of the eDNA and eRNA in the epididymal amyloid matrix including release from the seminiferous tubule epithelium in the testis, epididymal epithelium, spermatozoa, and/or pathogens. Because the mice were healthy with no obvious sign of epididymal infection, the contribution from pathogens is likely minimal. We used the DC1 mouse caput epididymal cell line to determine if the epididymal epithelial cells produce an eDNA/eRNA-containing amyloid matrix. The use of a cell line allowed us to establish the

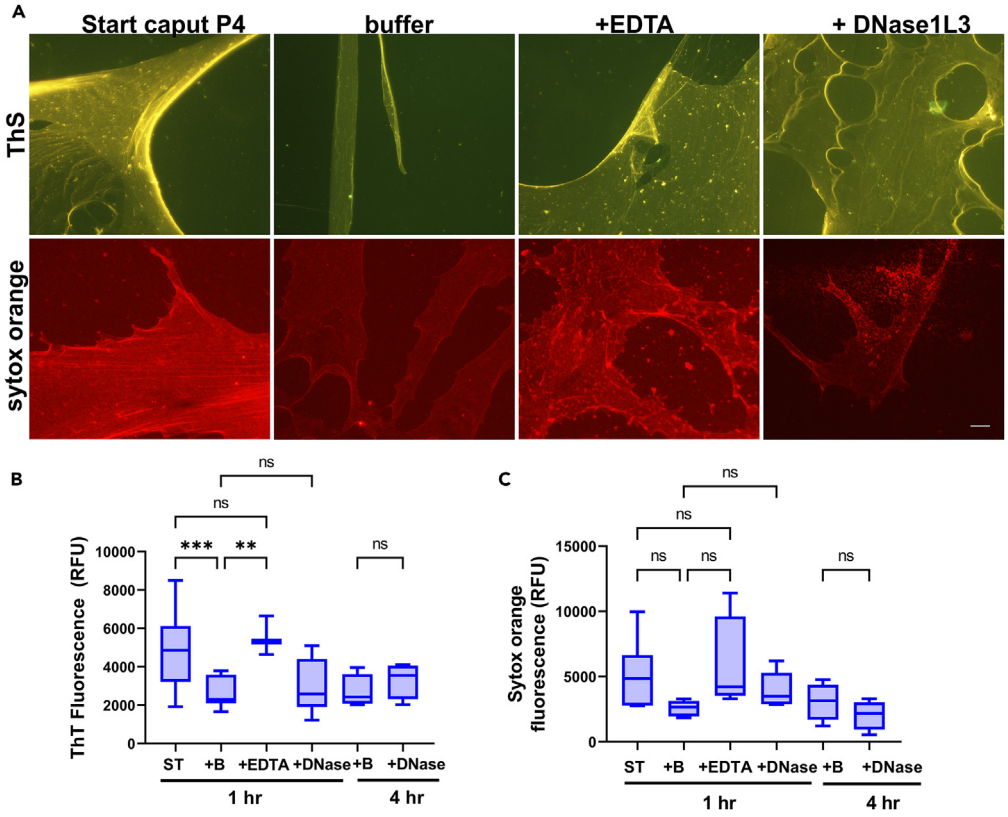

Figure 5. An endogenous activity partially disassembles the caput P4 epididymal amyloid matrix

(A) Caput P4 amyloid fractions (30 μg) were incubated with DNase buffer (buffer, B), DNase buffer + EDTA (+EDTA), or 5 μg/mL DNase1IL3 (+DNase1L3) for 1 h at 37°C. Start sample (ST) was caput P4 amyloid incubated in buffer without $MgCl_2$. Samples were dried overnight on a slide and incubated with ThS to visualize amyloid while a second set of samples were incubated with Sytox Orange to detect nucleic acids. Scale bar, 40 μM. See also Figure S2.

A proportion of each sample analyzed in A) was added to a 96 well plate in the presence of either B) 20 μM ThT or C) 0.2 μM Sytox Orange and relative fluorescence units measured with a Tecan plate reader. Caput P4 samples were also incubated for 4 h in DNase buffer only (+B) or DNase1L3 (+DNase). Data are represented as mean ± SEM from n = 3–9 experiments where each experiment used freshly isolated epididymal amyloid matrix. Statistical analyses were performed using ANOVA followed by multiple comparisons test in GraphPad Prism 9.5. $^{**}p = 0.002$, $^{***}p = 0.0005$. n.s., not significant. See also Figure S3.

presence of nucleic acids without the risk of contributions from spermatozoa. Cells were grown to confluency, conditioned media collected, and fractions containing P4 amyloids isolated as done with the epididymal amyloid matrix. As shown in Figure 8A, Sytox Orange fluorescence was detected in small particles in the P4 fraction while ThS was present in particles and a film-like structure, indicating the presence of nucleic acids within the epididymal epithelial cell amyloid matrix. Although the conditioned media was centrifuged several times to remove dead cells prior to isolating the P4 fraction, we cannot rule out that some nucleic acids in the conditioned media were released from these cells. Agarose gel electrophoresis analysis of total DC1 cell conditioned media (not centrifuged) and a P4 fraction isolated from the conditioned media, showed several populations of nucleic acids. These included a high molecular mass population that did not enter far into the ethidium bromide-stained gel, faint levels of intermediate (1.5–10 kb) forms and a smaller (~250 bp) form, populations like that observed in the P2 and P4 fractions from the caput epididymis (Figure 8B). Likewise, RNase caused the loss of the intermediate and smaller forms of nucleic acid with no effect on the high molecular mass population. Together, our data suggest the epididymal epithelial cells are a source of eDNA and eRNA in the mouse epididymal amyloid matrix.

Polysaccharides are a component of the epididymal amyloid matrix and contribute to matrix integrity

To determine if the epididymal amyloid matrix contains mucin-like polysaccharides, caput and cauda P4 amyloids were stained with wisteria floribunda agglutinin (WFA) which is used to identify N-acetylgalactosamines beta 1 (GalNAc) residues in mucin-like glycoproteins, including chondroitin sulfate proteoglycans.[40] Our experiments revealed that both the caput and cauda amyloid matrix contain complex GalNAc - containing sugars with the cauda P4 containing more GalNAc sugars compared to that in the caput P4 amyloid (Figure 9A, control). We next treated caput and cauda P4 amyloids with amylase, a glycoside hydrolase which breaks down the α-bonds of large α-linked polysaccharides into smaller oligosaccharides, and which is commonly used to digest bacterial biofilms.[41] Amylase digestion resulted in a decrease in WFA staining and a fragmentation of the WFA-stained caput and cauda P4 amyloid matrix confirming the presence of polysaccharides and their

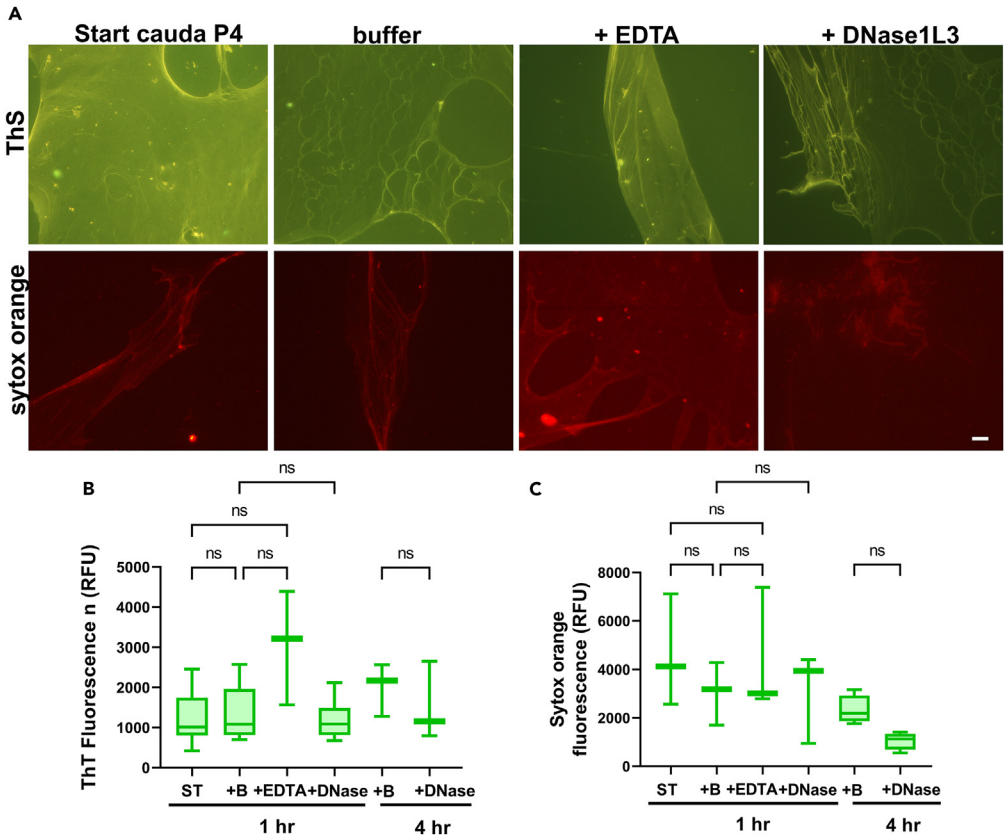

Figure 6. The cauda P4 amyloid matrix is resistant to disassembly

(A) Cauda P4 amyloid fractions (30 μg) were incubated with DNase buffer (buffer), DNase buffer + EDTA, and 5 μg/mL DNase1L3 for 1 h at 37°C. Start sample was cauda P4 amyloid incubated in buffer without $MgCl_2$. Samples were dried overnight on a slide and incubated with ThS to visualize amyloid while a second set of samples were incubated with Sytox Orange to detect nucleic acids. Images were captured using a Zeiss Axiovert 200M microscope equipped with epifluorescence. Scale bar, 40 μM.

A proportion of each sample analyzed in A) was added to a 96 well plate in the presence of either B) 20 μM ThT or C) 0.2 μM Sytox Orange and relative fluorescence units measured with a Tecan plate reader. Cauda P4 samples were also incubated for 4 h in DNase buffer only (+B) or DNase1L3 (+DNase). Data are represented as mean ± SEM from n = 3–9 experiments where each experiment used freshly isolated epididymal amyloid matrix. Statistical analyses were performed using ANOVA followed by multiple comparisons test in GraphPad Prism 9.5., n.s., not significant. See also Figure S3.

contribution to maintaining overall structure (Figure 9A). More profound effects of amylase were observed in the caput P4 amyloid compared to the cauda P4 amyloid, consistent with it containing less polysaccharide and thus possibly being more easily dispersed. In addition, the caput P4 amyloid fraction exhibited a significant decrease ($p < 0.05$) in amyloid content after exposure to amylase indicating a close association between the polysaccharide and amyloid components of the epididymal amyloid matrix (Figure 9B). A significant decrease in amyloid was not observed in the cauda P4 fraction even after 4 h of amylase exposure possibly due to greater amounts of polysaccharide protecting the amyloid and/or its higher ordered state (Figure 9B).

To confirm the presence of mucin-like polysaccharides, we stained whole epididymal tissue sections with Alcian blue pH 2.5 to detect acid mucins *in situ* including those with sulfated, carboxylic, hyaluronic, and chondroitin residues. Like that seen with WFA, more Alcian blue staining was observed in the cauda compared to the caput region indicative of more acidic mucin polysaccharides in the distal epididymis (Figure 10A). Some epididymal sections were also counterstained stained with neutral red that helped define structures in the epididymal lumen. The counterstained sections, which had a brown staining (red+blue), revealed a thin, branched matrix in the caput epididymal lumen that became a granular layer surrounding the spermatozoa and that continued into the cauda epididymal lumen (Figure 10A). Some sections also showed luminal patches of acid mucin polysaccharides with few spermatozoa suggesting the amyloid matrix is heterogeneous with distinct layers of sperm and polysaccharides distributed throughout the lumen (Figure 10A, *). Interestingly, in the cauda epididymal tubules we observed sperm organized into distinct mucin positive tunnels giving a swirled appearance (Figure S4). Whether a function of the mucin polysaccharide/amyloid matrix is to stratify the sperm into organized structures for storage in the cauda epididymis requires further study.

P4 amyloid fractions isolated from the caput and cauda luminal fluid were also stained with Alcian blue pH 2.5 to detect total acid mucins, pH1 to detect only sulfated acid mucins and pH 0.2 to detect strongly sulfated mucins. Alcian blue staining was observed at all pH conditions suggesting several types of acid mucins, including those that are strongly sulfated, are components of the epididymal amyloid matrix

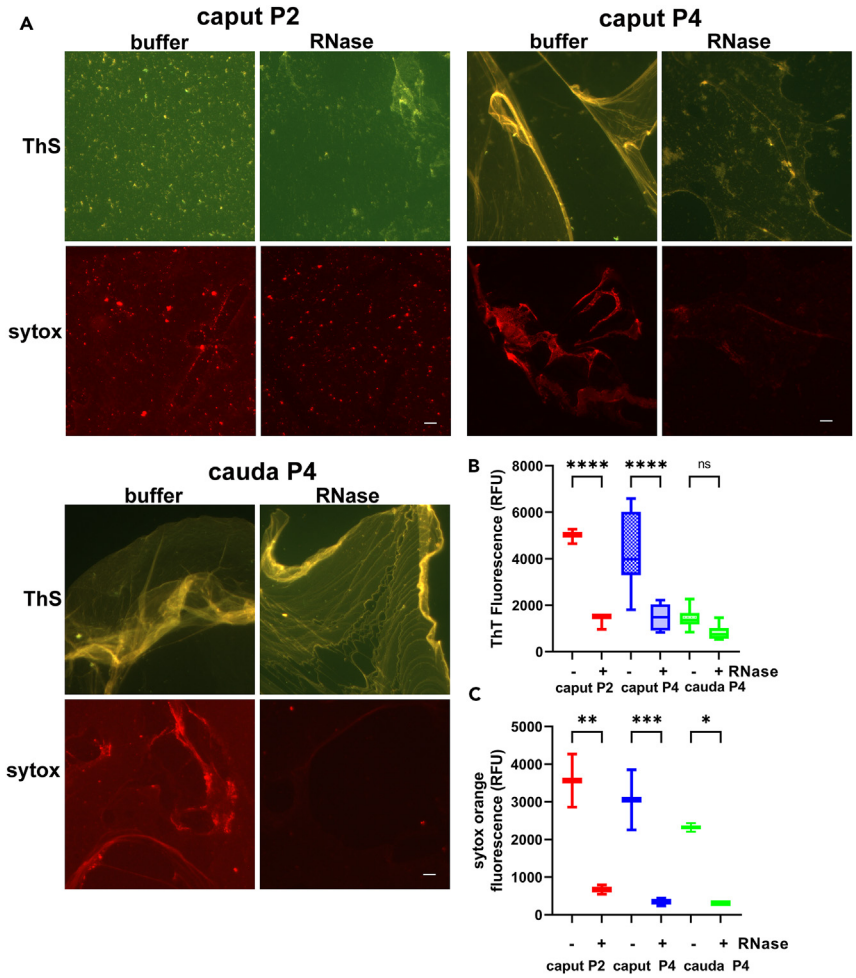

Figure 7. eRNA contributes to the maintenance of the epididymal amyloid matrix structure

(A) Caput P2, caput 4 and cauda P4 amyloid fractions were incubated with DNase-free RNase or buffer only for 30 min at 37°C, dried overnight on a slide and stained with ThS or Sytox Orange to detect amyloid and nucleic acids, respectively. Scale bar, 40 μm.

A proportion of each sample analyzed in A) was added to a 96 well plate in the presence of either B) 20 μM ThT or C) 0.2 μM Sytox Orange and relative fluorescence units measured with a Tecan plate reader. Data are represented as mean ± SEM from n = 3–4 experiments where each experiment used freshly isolated epididymal amyloid matrix. Statistical analyses were performed using ANOVA followed by multiple comparisons test in GraphPad Prism 9.5. *p = 0.017, **p = 0.002, ***p = 0.0008, ****p < 0.0001. n.s., not significant.

(Figure 10B). Together our studies show that mucin polysaccharides are a part of the amyloid matrix and contribute to the maintenance of its structure. Further, higher levels of polysaccharides are a characteristic of the cauda epididymal amyloids, which may be reflective of it being a more mature and established structure.

DISCUSSION

The epididymal amyloid matrix has the features of a bacterial biofilm

Here we show that the mouse epididymal amyloid matrix contains eDNA, eRNA, and complex polysaccharides, components that are critical for maintaining the extracellular epididymal amyloid matrix structure much like their functions in bacterial biofilms. Our previous work showing the epididymal amyloid matrix has host defense functions revealed a biological role similar to that of biofilms.[7] Together, our studies suggest evolutionarily conserved mechanisms underlie the assembly and function of highly specialized extracellular matrices (ECMs) that protect a bacterial community and the mammalian germ line. Other mammalian host defense structures such as gut α-defensin nanonets form an amyloid/eDNA structure to enable the trapping of the pathogen providing additional evidence of how nature has conserved some of the features of biofilm in higher organisms.[42] However, whether eRNA and polysaccharides are also functional components of these structures is not known. Nanonets are also distinct in that they form solely in response to a pathogen while the epididymal amyloid matrix is always present, including in the absence of infection, implying roles in addition to host defense.

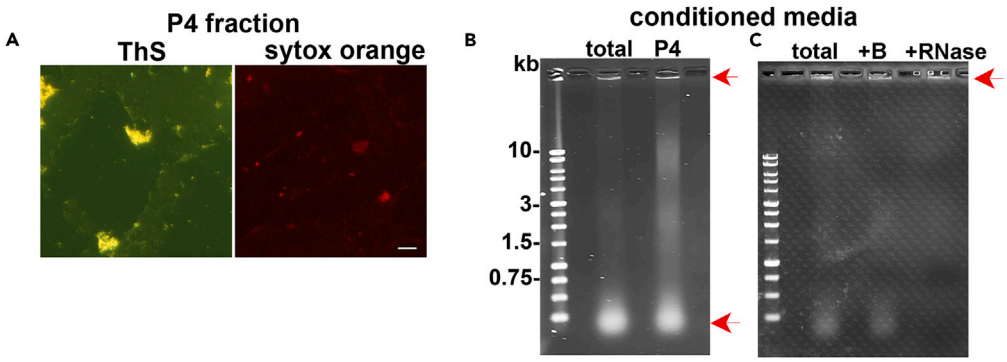

Figure 8. Epididymal epithelial cells are a source of nucleic acids in the epididymal amyloid matrix

(A) The P4 amyloid fraction was isolated from the conditioned media from the DC1 caput epididymal epithelial cell line and stained with Thioflavin S to detect amyloid and sytox orange to detect nucleic acid. Scale bar, 40 μm.

(B) Twenty μgs of DC1 cell conditioned media (total) and the isolated P4 fraction were examined by 1% agarose-TAE gel electrophoresis and EtBr staining. Red arrows indicate the high molecular mass population of eDNA and the 250 bp population of RNA.

(C) Twenty μgs of total DC1 cell conditioned media were incubated with RNase or buffer only (B) for 30 min at 37°C and examined by agarose gel electrophoresis and EtBr staining. Red arrow indicates the high molecular mass population of eDNA.

eDNA and eRNA are integral components of the epididymal amyloid matrix and exhibit behaviors like their counterparts in bacterial biofilm

We show that one role of the eDNA in the epididymal amyloid is to support the overall integrity of the structure since upon the activation of a putative endogenous nuclease activity the amyloid matrix developed large holes and became fragmented. Disruption of the amyloid matrix structure was noted especially in the caput P2 and P4 samples consistent with it being an immature structure still undergoing assembly in this region. The caput amyloid structure was also affected by exogenous RNase indicating both eDNA and eRNA are part of the epididymal amyloid matrix and required for maintenance of its structure. Although the discovery of eRNA in bacterial biofilms is relatively recent,[43,44] there is evidence of DNA/RNA-dependent biofilms. Studies in *Pseudomonas* in which eDNA was isolated from biofilms under conditions that maintained its *in vivo* biophysical properties revealed that purine-rich RNA was also present in the eDNA network.[25] These studies suggested that non-canonical base pair interactions between the RNA and DNA allowed the formation of a nucleic acid gel and the viscoelastic properties of the biofilm.

eDNA likely performs additional roles in the epididymal amyloid matrix as it does in bacterial biofilms. eDNA has been shown to template the assembly of amyloidogenic proteins, suggesting it may serve as an initiator in the formation of an amyloid infrastructure.[45] We have preliminary evidence that CRES, a component of the epididymal amyloid matrix, assembles into amyloid in the presence of DNA, a process that we speculate may initiate or contribute to the building of the structure (Cornwall unpublished). If so, some populations of eDNA may be integrated into the amyloid matrix such that they are partially protected from complete digestion or may be resistant to DNases. The cauda epididymal P4 amyloid, which our studies indicate is an advanced/mature amyloid structure compared to that in the caput epididymis, showed little to no changes in its structure in the presence of nucleases, a behavior comparable to the mature forms of many bacterial biofilms.[19,46] The similarity in behaviors between the cauda P4 amyloid and mature biofilms suggests common mechanisms for their enhanced stability.

The eDNA in some biofilms has been shown to be like intracellular DNA but with different methylation patterns.[47] However, other studies indicate biofilm eDNA has a different higher ordered structure than chromosomal DNA and often is in a stabilized noncanonical configuration. In *E.coli* and other bacteria, eDNA was shown to have a Holliday junction-like arrangement that was critical for biofilm structural and mechanical integrity.[20] Studies of *P. aeruginosa* eDNA showed that it formed G-quadruplexes, noncanonical secondary structures formed by G-rich sequences that contribute to the stability of the biofilm.[48] In some bacterial biofilms eDNA changes its structure from the right-handed nuclease sensitive B-DNA form, the most common DNA conformation in biological conditions, to a more stable and nuclease resistant left-handed Z-DNA conformation as the biofilm matures.[46] Altogether, the distinct and highly ordered structures of eDNA, and possibly also eRNA, in biofilms are thought to be mechanisms to allow the maturing biofilm to become more resistant to host responses providing further stability and protection for the bacterial colony. While studies are ongoing in our lab to determine if eDNA in the cauda P4 amyloid is in the Z conformation and/or has formed G-quadruplexes, it is possible such a transition might occur to enhance the stability of the amyloid matrix in the cauda epididymis which performs a critical role as a storage site for the mature spermatozoa.

The populations of eDNA and eRNA that we observed in the epididymal amyloid matrix exhibit sizes comparable with what has been detected in some biofilms; these include a high molecular mass population of eDNA (>10 kb) that does not migrate well into the gel and an eRNA population of ~250 bp.[43] In other biofilms, however, smaller eDNA fragments have been observed. In a hyperbioflm-forming clinical variant of *P. aeruginosa* the release of eDNA fragments (100 bp-12000bp) from a subpopulation of the bacteria enabled the biofilm to become resistant to DNase1 unlike the wildtype cells that released typical >10 kb eDNA forms.[49] These data suggest that eDNA itself may change in

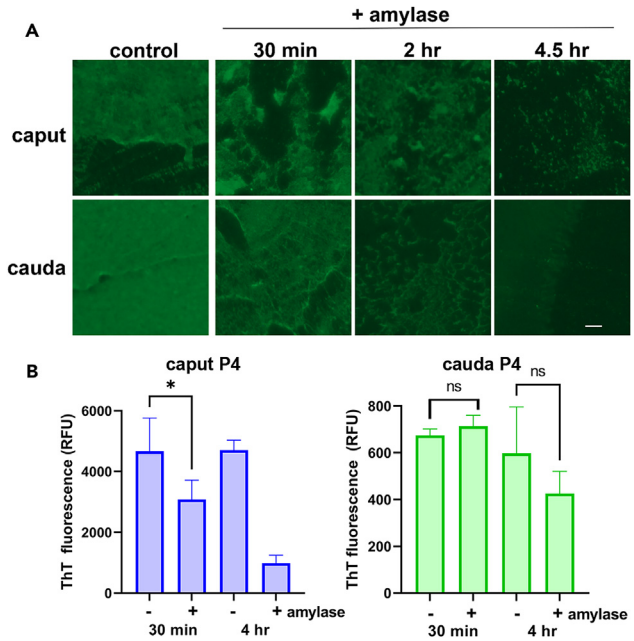

Figure 9. Mucin-like polysaccharides contribute to epididymal amyloid matrix integrity

(A) Caput and cauda P4 amyloid fractions were dried on a slide overnight and stained with wisteria floribunda agglutinin (WFA), a stain for N-acetylgalactosamine beta 1 residues, before (control) and after treatment with 0.1% amylase. Scale bar, 20 μm.

(B) Caput and cauda P4 amyloid fractions were incubated with 0.1% amylase and total amyloid levels were determined by ThT fluorescence after 30 min and 4 h. The relative ThT fluorescence units of control and amylase treated (except for caput P4 at 4 h) were compared by t-test using GraphPad Prism 9.5.1. Data are represented as mean ± SEM. $n = 3$ experiments for all samples except for caput P4 ± amylase at 4 h where $n = 2$. Each experiment used freshly isolated epididymal amyloid matrix. *, $p < 0.05$. n.s., not significant.

biofilms as an adaptive response to the environment resulting in an altered biofilm structure. Whether the >10 kb forms of eDNA observed in the epididymal amyloid matrix would change following an infection or an exposure to other environmental stressors, and if, and how, these changes might contribute to a changed epididymal amyloid matrix structure and function requires further investigation. In our previous studies, we observed that the epididymal amyloid matrix formed different amyloid structures with different host defense functions depending on the bacterial strain it encountered.[7] These results indicate the epididymal amyloid, such as biofilms, has an inherent ability to respond to environmental cues, which in part could be mediated by eDNA.

Source of nucleic acids in the epididymal amyloid matrix

Although our data suggest that epididymal epithelial cells are a source of eDNA and eRNA in the amyloid matrix produced *in vitro*, we cannot conclude that epithelial cells are the only source. In addition to the principal cells, the primary epithelial cell in the epididymis, there are other cell populations that could contribute nucleic acids including apical cells, clear cells, and basal cells. In addition, eDNA and eRNA could come from damaged spermatozoa or secretions from the testis and efferent ducts. Further studies are needed to determine the mechanisms by which nucleic acids become extracellular in the epididymal lumen. The release of DNA from bacteria is still under investigation but can include a suicidal programmed bacterial apoptosis or a fratricide-induced death or excretion from living cells.[50,51] eDNA in extracellular traps released by neutrophils (NETs) comes from that bound to histones through cell lysis and, occasionally, from mitochondrial DNA.[52,53] In addition to eDNA in the epididymal amyloid matrix, the caput and cauda epididymal P4 amyloid preparations likely contain extracellular vesicles/exosomes (EVs) and condensates which may contain DNA and RNA.[54,55] If so, EVs could be one mechanism by which epididymal cells provide eDNA and eRNA to the amyloid matrix; however, we think it likely other mechanisms are involved as well considering nucleic acids may be a part of the amyloid matrix infrastructure.

Polysaccharides contribute to the maintenance of the epididymal amyloid matrix structure

Our results show that polysaccharides are a component of the amyloid matrix throughout the epididymis with higher amounts present in the mature epididymal amyloid structure. Using wisteria floribunda agglutinin and Alcian blue staining we showed in the cauda epididymis and in isolated cauda P4 amyloid fractions robust levels of N-acetylgalactosamines beta 1 (GalNAc beta 1–3 Gal) residues that are present in a variety of glycoconjugates including sulfated and acid mucin-like polysaccharides. Similarly, sulfated glycosaminoglycans, alginate and other negatively and positively charged extracellular polymeric substances are key constituents of biofilms from a variety of environments.[27,56,57] These mucin-like sugars help create the stickiness or "glue" that holds the biofilm together. We observed the cauda epididymal P4 amyloid likewise

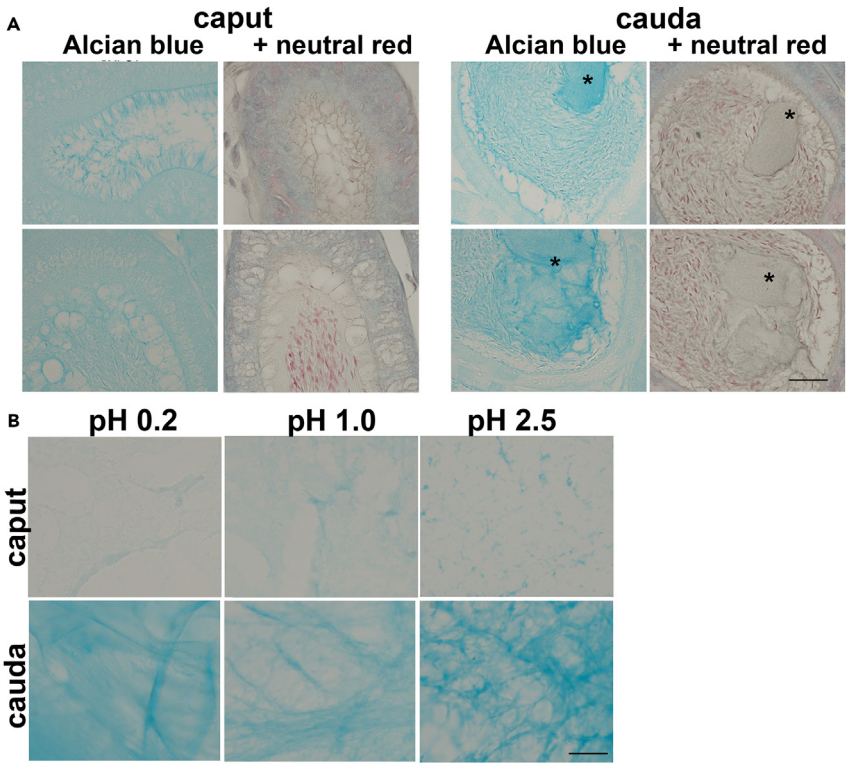

Figure 10. Acid mucin polysaccharides, including those strongly sulfated, are present in the epididymal amyloid matrix and enriched in the cauda epididymis

(A) Mouse epididymal tissue sections were stained with Alcian blue, pH 2.5 with and without counterstaining with neutral red to detect acid mucins including those with sulfated, carboxylic, hyaluronic, and chondroitin residues. More robust staining was detected in the cauda compared to the caput epididymis. Neutral red stains nuclei and lysosomes and as a counterstain helped reveal the mucin-rich amyloid matrix (blue + red = brown) surrounding spermatozoa. * Area of polysaccharides without spermatozoa.

(B) P4 amyloid fractions isolated from the caput and cauda epididymis were stained with Alcian blue at pH pH 2.5 to detect total acid mucins, pH 1 to detect only sulfated acid mucins and pH 0.2 to detect strongly sulfated acid mucins. Scale bar, 20 μm. See also Figure S4.

formed a sticky pellet during isolation that may be due to its mucin-like polysaccharides. Our data also showed that amylase treatment disrupted the caput P4 epididymal amyloid matrix indicating a role for polysaccharides in maintaining its integrity, like polysaccharide function in biofilms. The cauda P4 amyloid, however, was less affected by the amylase treatment than the caput possibly due to its higher polysaccharide content preventing significant change in amyloid content in the time frame of the amylase exposure. Alternatively, a more stable amyloid/eDNA/eRNA infrastructure in the cauda P4 epididymal amyloid prevented its disassembly.

Mucin-like sugars also contribute to the protective nature of biofilms by forming physical barriers and providing a tolerogenic environment for the immunogenic bacteria.[58] The epididymis must also maintain a tolerogenic environment for the naturally autoantigenic sperm. Although the mechanism by which the epididymis maintains tolerance is not known, our studies here showing parallels between the epididymal amyloid matrix and biofilms suggest that the thick mucin-like polysaccharide layer in the epididymal amyloid matrix could be integral for this protection.

Nucleases, amylase, and glucosidases in the epididymis and seminal fluid: regulation of epididymal amyloid matrix assembly/disassembly?

Nucleases with distinct DNA and RNA digesting activities have been described in the epididymal lumen but their biological functions remain unclear. These include a novel nuclease that requires Ca++-chelated EGTA for its degradation of DNA and is proposed to function in the apoptotic degradation of sperm chromatin[38] and RNAse T2 that when overexpressed in the epididymis leads to altered small noncoding RNAs.[39] DNase(s) in seminal plasma include types I and II[59] such as bovine sperm fertility associated antigen that has 88% identity with human DNase1L3.[60] DNases in seminal fluid have been used as a marker for fertility in large mammals, as increased levels of DNase are correlated with a higher rate of successful fertilization.[61] However, the fact that nature would intentionally surround spermatozoa, whose sole function is to provide DNA for the next generation, with DNases seems inherently risky.

We speculate nucleases have several roles in the male reproductive tract. Because eDNA is known to template amyloid assembly, distinct, and likely tightly controlled, DNases may be present within the epididymal lumen to regulate the epididymal amyloid matrix,

including its possible remodeling, by controlling the amount or location of template eDNA. Further studies are needed to establish the identities of epididymal nucleases including if DNAse1L3 is present in the epididymal lumen. Seminal plasma DNases may help disassemble the epididymal amyloid matrix after ejaculation allowing the sperm to swim up the female tract for fertilization. Indeed, cell-free DNA, single and double-stranded RNA, and small RNAs (miRNA and piRNA) have been found in human semen.[62–65] Whether the nucleic acids represent that released from digested epididymal amyloid matrix or damaged spermatozoa, secreted from other male tract organs such as prostate or seminal vesicle for distinct biological roles, or a combination thereof remains to be determined. In addition to DNase activity, seminal fluid contains amylase and α-glucosidase, both of which have been used as fertility markers and are known to assist in the liquefaction of semen.[66,67] Amylase treatment has also been used to increase fertilization rates in men.[68] Although, α-glucosidase is made and stored in the epididymis it does not appear to be active until the seminal fluid, which would be appropriate if its role was to help disassemble the epididymal amyloid matrix.[67] Thus, while in our studies nucleases and amylase, individually only partially disrupted the caput epididymal amyloid matrix with less influence on the cauda amyloid matrix, their combined activities in the seminal plasma, along with other components such as glucosidases, might be sufficient to disassemble the structure and allow the release of spermatozoa. If so, higher levels of DNase and/or amylase in semen would likely result in increased fertility because of enhanced amyloid matrix disassembly.

Together, our studies show structural and functional relationships between a specialized ECM that surrounds the maturing mammalian spermatozoa and an ECM that surrounds a bacterial community suggesting evolutionarily conserved mechanisms for their assembly and functions. In addition to providing clues of how the epididymal amyloid matrix protects the germ line from pathogens, knowledge of how biofilms interact with and "nurture" a bacterial community may be helpful for understanding basic mechanisms of sperm maturation. Correspondingly, this knowledge also could help identify underlying mechanisms of idiopathic male infertility because of an altered epididymal amyloid matrix.

Limitations of the study

In the present study we show the epididymal amyloid matrix has structural and functional properties like that of bacterial biofilms. A limitation of this work is that some of our analyses required amyloid matrix isolated from the mouse epididymis rather than the examination of the structure *in situ*. It is possible that some eDNA/eRNA observed in the amyloid matrix represents that released from epididymal epithelial cells or spermatozoa damaged during the amyloid matrix isolation procedure. Our studies showing that DNase buffer ($MgCl_2$) caused the epididymal amyloid matrix to form clear zones suggest the presence of an endogenous Mg-dependent nuclease and/or protease activity. Further studies are needed however, to establish the underlying mechanism resulting in the change in amyloid matrix structure including whether this represents a direct unwinding of amyloid/protein and/or effects on nucleic acids. Further studies are also needed to establish how eDNA/eRNA, CRES subgroup amyloids, proteoglycans, and possibly other components, assemble into the epididymal amyloid matrix.

STAR★METHODS

Detailed methods are provided in the online version of this paper and include the following:

- KEY RESOURCES TABLE
- RESOURCE AVAILABILITY
  - Lead contact
  - Materials availability
  - Data and code availability
- EXPERIMENTAL MODEL AND STUDY PARTICIPANT DETAILS
  - Animals
  - Cell culture
- METHOD DETAILS
  - Isolation of epididymal amyloid fractions
  - Nucleic acid and Thioflavin S staining
  - Preparation of human DNAse1L3, DNase, and RNase treatment of epididymal amyloids
  - Amylase treatment and wisteria floribunda agglutinin staining
  - Alcian blue staining
  - Collection of conditioned media
  - Examination of nucleic acids by agarose gel electrophoresis
  - Plasmid digestion assay
  - Epididymal amyloid matrix degradation assay
- QUANTIFICATION AND STATISTICAL ANALYSIS

SUPPLEMENTAL INFORMATION

Supplemental information can be found online at https://doi.org/10.1016/j.isci.2024.110152.

ACKNOWLEDGMENTS

Supported in part by TTUHSC (GAC), the Newby Family (GAC), and the Lupus Research Alliance (RBS).

AUTHOR CONTRIBUTIONS

C.M., G.R.A., and G.A.C. designed and performed the experiments, J.V. and R.B.S. contributed reagents, C.M., G.R.A., and G.A.C., interpreted the results, C.M., J.V., and G.A.C. wrote the article. All authors contributed to the article.

DECLARATION OF INTERESTS

The authors declare no competing interests.

Received: December 1, 2023
Revised: April 14, 2024
Accepted: May 28, 2024
Published: May 31, 2024

REFERENCES

1. Tung, K.S.K., Harakal, J., Qiao, H., Rival, C., Li, J.C.H., Paul, A.G.A., Wheeler, K., Pramoonjago, P., Grafer, C.M., Sun, W., et al. (2017). Egress of sperm autoantigen from seminiferous tubules maintains systemic tolerance. J. Clin. Invest. *127*, 1046–1060. https://doi.org/10.1172/JCI89927.
2. Wheeler, K., Tardif, S., Rival, C., Luu, B., Bui, E., Del Rio, R., Teuscher, C., Sparwasser, T., Hardy, D., and Tung, K.S.K. (2011). Regulatory T cells control tolerogenic versus autoimmune response to sperm in vasectomy. Proc. Natl. Acad. Sci. USA *108*, 7511–7516. https://doi.org/10.1073/pnas.1017615108.
3. Whelly, S., Johnson, S., Powell, J., Borchardt, C., Hastert, M.C., and Cornwall, G.A. (2012). Nonpathological extracellular amyloid is present during normal epididymal sperm maturation. PLoS One *7*, e36394. https://doi.org/10.1371/journal.pone.0036394.
4. Whelly, S., Muthusubramanian, A., Powell, J., Johnson, S., Hastert, M.C., and Cornwall, G.A. (2016). Cystatin-related epididymal spermatogenic subgroup members are part of an amyloid matrix and associated with extracellular vesicles in the mouse epididymal lumen. Mol. Hum. Reprod. *22*, 729–744. https://doi.org/10.1093/molehr/gaw049.
5. Cornwall, G.A., and Hsia, N. (2003). A new subgroup of the family 2 cystatins. Mol. Cell. Endocrinol. *200*, 1–8. https://doi.org/10.1016/s0303-7207(02)00408-2.
6. Do, H.Q., Hewetson, A., Borcik, C.G., Hastert, M.C., Whelly, S., Wylie, B.J., Sutton, R.B., and Cornwall, G.A. (2020). Cross-seeding between the functional amyloidogenic CRES and CRES3 family members and their regulation of Ab assembly. J. Biol. Chem. *296*, 100250. https://doi.org/10.1074/jbc.RA120.015307.
7. Myers, C., Hastert, M.C., and Cornwall, G.A. (2022). Host defense functions of the epididymal amyloid matrix. Mol. Hum. Reprod. *28*, gaac038. https://doi.org/10.1093/molehr/gaac038.
8. Chapman, M.R., Robinson, L.S., Pinkner, J.S., Roth, R., Heuser, J., Hammar, M., Normark, S., and Hultgren, S.J. (2002). Role of Escherichia coli curli operons in directing amyloid fiber formation. Science *295*, 851–855. https://doi.org/10.1126/science.1067484.
9. Wang, X., and Chapman, M.R. (2008). Curli provide the template for understanding controlled amyloid propagation. Prion *2*, 57–60. https://doi.org/10.4161/pri.2.2.6746.
10. Bowden, G.H., and Li, Y.H. (1997). Nutritional influences on biofilm development. Adv. Dent. Res. *11*, 81–99. https://doi.org/10.1177/08959374970110012101.
11. Sharma, D., Misba, L., and Khan, A.U. (2019). Antibiotics versus biofilm: an emerging battleground in microbial communities. Antimicrob. Resist. Infect. Control *8*, 76. https://doi.org/10.1186/s13756-019-0533-3.
12. Jiang, Y., Geng, M., and Bai, L. (2020). Targeting Biofilms Therapy: Current Research Strategies and Development Hurdles. Microorganisms *8*, 1222. https://doi.org/10.3390/microorganisms8081222.
13. Flemming, H.C., Neu, T.R., and Wozniak, D.J. (2007). The EPS matrix: the "house of biofilm cells". J. Bacteriol. *189*, 7945–7947. https://doi.org/10.1128/JB.00858-07.
14. Akbey, Ü., and Andreasen, M. (2022). Functional amyloids from bacterial biofilms - structural properties and interaction partners. Chem. Sci. *13*, 6457–6477. https://doi.org/10.1039/d2sc00645f.
15. Van Gerven, N., Van der Verren, S.E., Reiter, D.M., and Remaut, H. (2018). The Role of Functional Amyloids in Bacterial Virulence. J. Mol. Biol. *430*, 3657–3684.
16. Vidakovic, L., Singh, P.K., Hartmann, R., Nadell, C.D., and Drescher, K. (2018). Dynamic biofilm architecture confers individual and collective mechanisms of viral protection. Nat. Microbiol. *3*, 26–31. https://doi.org/10.1038/s41564-017-0050-1.
17. Whitchurch, C.B., Tolker-Nielsen, T., Ragas, P.C., and Mattick, J.S. (2002). Extracellular DNA required for bacterial biofilm formation. Science *295*, 1487. https://doi.org/10.1126/science.295.5559.1487.
18. Berne, C., Kysela, D.T., and Brun, Y.V. (2010). A bacterial extracellular DNA inhibits settling of motile progeny cells within a biofilm. Mol. Microbiol. *77*, 815–829. https://doi.org/10.1111/j.1365-2958.2010.07267.x.
19. Whitchurch, C.B., Tolker-Nielsen, T., Ragas, P.C., and Mattick, J.S. (2002). Extracellular DNA required for bacterial biofilm formation. Science *295*, 1487. https://doi.org/10.1126/science.295.5559.1487.
20. Devaraj, A., Buzzo, J.R., Mashburn-Warren, L., Gloag, E.S., Novotny, L.A., Stoodley, P., Bakaletz, L.O., and Goodman, S.D. (2019). The extracellular DNA lattice of bacterial biofilms is structurally related to Holliday junction recombination intermediates. Proc. Natl. Acad. Sci. USA *116*, 25068–25077. https://doi.org/10.1073/pnas.1909017116.
21. Secchi, E., Savorana, G., Vitale, A., Eberl, L., Stocker, R., and Rusconi, R. (2022). The structural role of bacterial eDNA in the formation of biofilm streamers. Proc. Natl. Acad. Sci. USA *119*, e2113723119. https://doi.org/10.1073/pnas.2113723119.
22. Das, T., Sharma, P.K., Busscher, H.J., van der Mei, H.C., and Krom, B.P. (2010). Role of extracellular DNA in initial bacterial adhesion and surface aggregation. Appl. Environ. Microbiol. *76*, 3405–3408. https://doi.org/10.1128/AEM.03119-09.
23. Molin, S., and Tolker-Nielsen, T. (2003). Gene transfer occurs with enhanced efficiency in biofilms and induces enhanced stabilisation of the biofilm structure. Curr. Opin. Biotechnol. *14*, 255–261. https://doi.org/10.1016/s0958-1669(03)00036-3.
24. Chiang, W.C., Nilsson, M., Jensen, P.Ø., Høiby, N., Nielsen, T.E., Givskov, M., and Tolker-Nielsen, T. (2013). Extracellular DNA shields against aminoglycosides in Pseudomonas aeruginosa biofilms. Antimicrob. Agents Chemother. *57*, 2352–2361. https://doi.org/10.1128/AAC.00001-13.
25. Seviour, T., Winnerdy, F.R., Wong, L.L., Shi, X., Mugunthan, S., Castaing, R., Adav, R.S., Kohli, G.S., Shewan, H.M., Stokes, J.R., et al. (2020). The biofilm matrix scaffold of Pseudomonas species contains non-canonically base paired extracellular DNA and RNA. Preprint at bioRxiv. https://doi.org/10.1101/527267.
26. Mitra, A., and Mukhopadhyay, S. (2023). Regulation of biofilm formation by non-coding RNA in prokaryotes. Curr. Res. Pharmacol. Drug Discov. *4*, 100151.
27. Limoli, D.H., Jones, C.J., and Wozniak, D.J. (2015). Bacterial Extracellular Polysaccharides in Biofilm Formation and Function. Microbiol. Spectr. *3*. https://doi.org/10.1128/microbiolspec.MB-0011-2014.
28. Lahiri, D., Nag, M., Banerjee, R., Mukherjee, D., Garai, S., Sarkar, T., Dey, A., Sheikh, H.I., Pathak, S.K., Edinur, H.A., et al. (2021). Amylases: Biofilm Inducer or Biofilm Inhibitor? Front. Cell. Infect. Microbiol. *11*, 660048. https://doi.org/10.3389/fcimb.2021.660048.

29. Singh, S., Almuhanna, Y., Alshahrani, M.Y., Lowman, D.W., Rice, P.J., Gell, C., Ma, Z., Graves, B., Jackson, D., Lee, K., et al. (2021). Carbohydrates from Pseudomonas aeruginosa biofilms interact with immune C-type lectins and interfere with their receptor function. NPJ Biofilms Microbiomes *7*, 87. https://doi.org/10.1038/s41522-021-00257-w.
30. Overhage, J., Schemionek, M., Webb, J.S., and Rehm, B.H.A. (2005). Expression of the psl operon in Pseudomonas aeruginosa PAO1 biofilms: PslA performs an essential function in biofilm formation. Appl. Environ. Microbiol. *71*, 4407–4413. https://doi.org/10.1128/AEM.71.8.4407-4413.2005.
31. Henke, M.T., Brown, E.M., Cassilly, C.D., Vlamakis, H., Xavier, R.J., and Clardy, J. (2021). Capsular polysaccharide correlates with immune response to the human gut microbe Ruminococcus gnavus. Proc. Natl. Acad. Sci. USA *118*, e2007595118. https://doi.org/10.1073/pnas.2007595118.
32. Peng, N., Cai, P., Mortimer, M., Wu, Y., Gao, C., and Huang, Q. (2020). The exopolysaccharide-eDNA interaction modulates 3D architecture of Bacillus subtilis biofilm. BMC Microbiol. *20*, 115. https://doi.org/10.1186/s12866-020-01789-5.
33. Bravo, R., Arimon, M., Valle-Delgado, J.J., García, R., Durany, N., Castel, S., Cruz, M., Ventura, S., and Fernàndez-Busquets, X. (2008). Sulfated polysaccharides promote the assembly of amyloid beta(1-42) peptide into stable fibrils of reduced cytotoxicity. J. Biol. Chem. *283*, 32471–32483. https://doi.org/10.1074/jbc.M709870200.
34. Scholtmeijer, K., de Vocht, M.L., Rink, R., Robillard, G.T., and Wösten, H.A.B. (2009). Assembly of the Fungal SC3 Hydrophobin into Functional Amyloid Fibrils Depends on Its Concentration and Is Promoted by Cell Wall Polysaccharides. J. Biol. Chem. *284*, 26309–26314. https://doi.org/10.1074/jbc.M109.005553.
35. Michel, V., Duan, Y., Stoschek, E., Bhushan, S., Middendorff, R., Young, J.M., Loveland, K.L., Kretser, D.M.D., Hedger, M.P., and Meinhardt, A. (2016). Uropathogenic Escherichia coli causes fibrotic remodelling of the epididymis. J. Pathol. *240*, 15–24. https://doi.org/10.1002/path.4748.
36. McCord, J.J., Engavale, M., Masoumzadeh, E., Villarreal, J., Mapp, B., Latham, M.P., Keyel, P.A., and Sutton, R.B. (2022). Structural features of Dnase1L3 responsible for serum antigen clearance. Commun. Biol. *5*, 825. https://doi.org/10.1038/s42003-022-03755-5.
37. McCord, J.J., Engavale, M., Masoumzadeh, E., Villarreal, J., Mapp, B., Latham, M., Keyel, P., and Sutton, R.B. (2022). Structural features of Dnase1L3 responsible for diverse antigenic serum DNA clearance. Biophys. J. *121*, 442A.
38. Dominguez, K., and Ward, W.S. (2009). A Novel Nuclease Activity that is Activated by Ca2+ Chelated to EGTA. Syst. Biol. Reprod. Med. *55*, 193–199. https://doi.org/10.3109/19396360903234052.
39. Ma, Z., Li, J., Fu, L., Fu, R., Tang, N., Quan, Y., Xin, Z., Ding, Z., and Liu, Y. (2023). Epididymal RNase T2 contributes to astheno-teratozoospermia and intergenerational metabolic disorder through epididymosome-sperm interaction. BMC Med. *21*, 453. https://doi.org/10.1186/s12916-023-03158-1.
40. Hilbig, H., Bidmon, H.J., Blohm, U., and Zilles, K. (2001). Wisteria floribunda agglutinin labeling patterns in the human cortex: a tool for revealing areal borders and subdivisions in parallel with immunocytochemistry. Anat. Embryol. *203*, 45–52. https://doi.org/10.1007/s004290000135.
41. Craigen, B., Dashiff, A., and Kadouri, D.E. (2011). The Use of Commercially Available Alpha-Amylase Compounds to Inhibit and Remove Staphylococcus aureus Biofilms. Open Microbiol. J. *5*, 21–31.
42. Chu, H., Pazgier, M., Jung, G., Nuccio, S.P., Castillo, P.A., de Jong, M.F., Winter, M.G., Winter, S.E., Wehkamp, J., Shen, B., et al. (2012). Human alpha-Defensin 6 Promotes Mucosal Innate Immunity Through Self-Assembled Peptide Nanonets. Science *337*, 477–481. https://doi.org/10.1126/science.1218831.
43. Chiba, A., Seki, M., Suzuki, Y., Kinjo, Y., Mizunoe, Y., and Sugimoto, S. (2022). *Staphylococcus aureus* utilizes environmental RNA as a building material in specific polysaccharide-dependent biofilms. NPJ Biofilms Microbiomes *8*, 17. https://doi.org/10.1038/s41522-022-00278-z.
44. Flemming, H.C., Wingender, J., Szewzyk, U., Steinberg, P., Rice, S.A., and Kjelleberg, S. (2016). Biofilms: an emergent form of bacterial life. Nat. Rev. Microbiol. *14*, 563–575. https://doi.org/10.1038/nrmicro.2016.94.
45. Di Domizio, J., Zhang, R., Stagg, L.J., Gagea, M., Zhuo, M., Ladbury, J.E., and Cao, W. (2012). Binding with Nucleic Acids or Glycosaminoglycans Converts Soluble Protein Oligomers to Amyloid. J. Biol. Chem. *287*, 736–747. https://doi.org/10.1074/jbc.M111.238477.
46. Buzzo, J.R., Devaraj, A., Gloag, E.S., Jurcisek, J.A., Robledo-Avila, F., Kesler, T., Wilbanks, K., Mashburn-Warren, L., Balu, S., Wickham, J., et al. (2021). Z-form extracellular DNA is a structural component of the bacterial biofilm matrix. Cell *184*, 5740–5758.e17. https://doi.org/10.1016/j.cell.2021.10.010.
47. Miller, A.L., de Anda, J., Wong, G.C.L., and Tükel, Ç. (2022). Amyloid-containing biofilms and autoimmunity. Curr. Opin. Struct. Biol. *75*, 102435. https://doi.org/10.1016/j.sbi.2022.102435.
48. Seviour, T., Winnerdy, F.R., Wong, L.L., Shi, X., Mugunthan, S., Foo, Y.H., Castaing, R., Adav, S.S., Subramoni, S., Kohli, G.S., et al. (2021). The biofilm matrix scaffold of Pseudomonas aeruginosa contains G-quadruplex extracellular DNA structures. NPJ Biofilms Microbiomes *7*, 27. https://doi.org/10.1038/s41522-021-00197-5.
49. Deng, B., Ghatak, S., Sarkar, S., Singh, K., Das Ghatak, P., Mathew-Steiner, S.S., Roy, S., Khanna, S., Wozniak, D.J., McComb, D.W., and Sen, C.K. (2020). Novel Bacterial Diversity and Fragmented eDNA Identified in Hyperbiofilm-Forming Pseudomonas aeruginosa Rugose Small Colony Variant. iScience *23*, 100827. https://doi.org/10.1016/j.isci.2020.100827.
50. Yaron, S., Kolling, G.L., Simon, L., and Matthews, K.R. (2000). Vesicle-mediated transfer of virulence genes from Escherichia coli O157:H7 to other enteric bacteria. Appl. Environ. Microbiol. *66*, 4414–4420. https://doi.org/10.1128/AEM.66.10.4414-4420.2000.
51. Thomas, V.C., and Hancock, L.E. (2009). Suicide and fratricide in bacterial biofilms. Int. J. Artif. Organs *32*, 537–544. https://doi.org/10.1177/039139880903200902.
52. McIlroy, D.J., Jarnicki, A.G., Au, G.G., Lott, N., Smith, D.W., Hansbro, P.M., and Balogh, Z.J. (2014). Mitochondrial DNA neutrophil extracellular traps are formed after trauma and subsequent surgery. J. Crit. Care *29*, 1133.e1–1133.e5. https://doi.org/10.1016/j.jcrc.2014.07.013.
53. Brinkmann, V., Reichard, U., Goosmann, C., Fauler, B., Uhlemann, Y., Weiss, D.S., Weinrauch, Y., and Zychlinsky, A. (2004). Neutrophil extracellular traps kill bacteria. Science *303*, 1532–1535. https://doi.org/10.1126/science.1092385.
54. Sullivan, R. (2015). Epididymosomes: a heterogeneous population of microvesicles with multiple functions in sperm maturation and storage. Asian J. Androl. *17*, 726–729. https://doi.org/10.4103/1008-682X.155255.
55. Ghanam, J., Chetty, V.K., Barthel, L., Reinhardt, D., Hoyer, P.F., and Thakur, B.K. (2022). DNA in extracellular vesicles: from evolution to its current application in health and disease. Cell Biosci. *12*, 37. https://doi.org/10.1186/s13578-022-00771-0.
56. de Bruin, S., Vasquez-Cardenas, D., Sarbu, S.M., Meysman, F.J.R., Sousa, D.Z., van Loosdrecht, M.C.M., and Lin, Y. (2022). Sulfated glycosaminoglycan-like polymers are present in an acidophilic biofilm from a sulfidic cave. Sci. Total Environ. *829*, 154472. https://doi.org/10.1016/j.scitotenv.2022.154472.
57. Maunders, E., and Welch, M. (2017). Matrix exopolysaccharides; the sticky side of biofilm formation. FEMS Microbiol. Lett. *364*, fnx120. https://doi.org/10.1093/femsle/fnx120.
58. Farber, B.F., Kaplan, M.H., and Clogston, A.G. (1990). Staphylococcus epidermidis extracted slime inhibits the antimicrobial action of glycopeptide antibiotics. J. Infect. Dis. *161*, 37–40. https://doi.org/10.1093/infdis/161.1.37.
59. Quinn, P.J. (1968). Deoxyribonuclease activity in semen. J. Reprod. Fertil. *17*, 35–39.
60. McCauley, T.C., Buck, R.L., Marks, S.H., and Ax, R.L. (2008). Recombinant human seminal DNase. Biol. Reprod. *78*, 212.
61. Alghamdi, A.S., Funnell, B.J., Bird, S.L., Lamb, G.C., Rendahl, A.K., Taube, P.C., and Foster, D.N. (2010). Comparative studies on bull and stallion seminal DNase activity and interaction with semen extender and spermatozoa. Anim. Reprod. Sci. *121*, 249–258. https://doi.org/10.1016/j.anireprosci.2010.06.003.
62. Li, H., Huang, S., Guo, C., Guan, H., and Xiong, C. (2012). Cell-Free Seminal mRNA and MicroRNA Exist in Different Forms. PLoS One *7*, e34566. https://doi.org/10.1371/journal.pone.0034566.
63. Li, H.G., Huang, S.Y., Zhou, H., Liao, A.H., and Xiong, C.L. (2009). Quick recovery and characterization of cell-free DNA in seminal plasma of normozoospermia and azoospermia: implications for non-invasive genetic utilities. Asian J. Androl. *11*, 703–709. https://doi.org/10.1038/aja.2009.65.
64. Hu, L., Wu, C., Guo, C., Li, H., and Xiong, C. (2014). Identification of microRNAs predominately derived from testis and epididymis in human seminal plasma. Clin. Biochem. *47*, 967–972. https://doi.org/10.1016/j.clinbiochem.2013.11.009.
65. Zagoskin, M.V., Davis, R.E., and Mukha, D.V. (2017). Double Stranded RNA in Human Seminal Plasma. Front. Genet. *8*, 154. https://doi.org/10.3389/fgene.2017.00154.

66. Povoa, H. (1963). Amylase in human semen. J. Urol. *89*, 260–261.

67. Peña, P., Risopatrón, J., Villegas, J., Miska, W., Schill, W.B., and Sánchez, R. (2004). Alpha-glucosidase in the human epididymis:: topographic distribution and clinical application. Andrologia *36*, 315–320. https://doi.org/10.1111/j.1439-0272.2004.00625.x.

68. Dougherty, K.A., Cockett, A.T., and Urry, R.L. (1978). Effect of amylase on sperm motility and viability. J. Urol. *120*, 425–426.

69. Araki, Y., Suzuki, K., Matusik, R.J., Obinata, M., and Orgebin-Crist, M.C. (2002). Immortalized epididymal cell lines from transgenic mice overexpressing temperature-sensitive simian virus 40 large T-antigen gene. J. Androl. *23*, 854–869.

STAR★METHODS

KEY RESOURCES TABLE

REAGENT or RESOURCE	SOURCE	IDENTIFIER
Biological samples		
fetal bovine serum	R&D Systems	cat# S11150
Chemicals, peptides, and recombinant proteins		
thioflavin S	Sigma-Aldrich	cat# T1892
thioflavin T	Sigma-Aldrich	cat# T3516
Sytox Green	Invitrogen	cat# S7020
Sytox Orange	Invitrogen	cat# S11368
propidium idodide	Molecular Probes	cat# P134MP
Hoechst 33342	Thermo Scientific	cat# 62249
TOTO-3 iodide	Invitrogen	cat# T3604
Dulbeccos PBS	Sigma-Aldrich	cat# D5773
alcian blue	Sigma-Aldrich	cat#A5268
Supersignal West Pico Plus chemiluminescence substrate	Thermo Fisher Scientific	cat# 34580
neutral red	Sigma-Aldrich	cat# 72210
wisteria floribunda agglutinin-FITC	Invitrogen	cat# L32481
SUPERase-in RNase inhibitor	Invitrogen	cat# AM2696
RNase, DNase-free	Roche Diagnostics	cat# 11119915001
DNAse1, RNase-free	Roche Diagnostics	cat# 04716728001
alpha-amylase	MP Biomedicals	cat# 100447
Experimental models: Cell lines		
DC1 mouse epididymal cell line	generated and shared by M.C. Orgebin-Crist, Vanderbilt University	N/A
Experimental models: Organisms/strains		
Mice	Charles River	Crl:CD-1(ICR)
Software and algorithms		
GraphPad	Prism	version 9.5.1

RESOURCE AVAILABILITY

Lead contact

Further information and requests for resources and reagents should be directed to and will be fulfilled by the lead contact, Gail Cornwall (gail.cornwall@ttuhsc.edu).

Materials availability

This study did not generate new unique reagents.

Data and code availability

- All data reported in this paper will be shared by the lead contact upon request.
- This paper does not report original code.
- Any additional information required to reanalyze the data reported in this paper is available from the lead contact upon request.

EXPERIMENTAL MODEL AND STUDY PARTICIPANT DETAILS

Animals

Male CD1 mice (22-34 weeks of age) were obtained from Charles River (Wilmington, MA) and group housed under a constant 12 h light/12 h dark cycle with food and water *ad libitum*. Nestlets were provided for nesting. Two mice were used for each experiment. All animal studies

were conducted in accordance with the NIH Guidelines for the Care and Use of Experimental Animals using protocol #94041 approved by the Texas Tech University Health Sciences Center Institutional Animal Care and Use Committee.

Cell culture

The DC1 epididymal epithelial cell line (obtained from M. C. Orgebin-Crist[69]) was cultured in 10 cm dishes (Nuncleon, ThermoScientific)) at 37°C in 5% CO_2 in a humidified incubator in IMDM with phenol red supplemented with 10% fetal bovine serum (FBS) (R&D systems, Minneapolis, MN), 1mM sodium pyruvate, 0.1mM MEM non-essential amino acids, 4mM L-glutamine, 42 U/ml penicillin, 42 μg/ml streptomycin, and 0.001μM 5α-dihydrotestosterone (in 100% EtOH).

METHOD DETAILS

Isolation of epididymal amyloid fractions

The luminal contents from the caput and corpus-cauda epididymis were isolated by puncturing the tissue in 400 μl Dulbecco's PBS (dPBS) or 25 mM HEPES, pH 7.4, using a 30G needle and allowing material to disperse for 15 min at room temperature. The tissue was discarded and the sperm suspensions were centrifuged at 500 x g for 5 min to remove spermatozoa (P1). The S1 supernatant was spun again to remove any remaining spermatozoa and then centrifuged at 5000 x g for 10 minutes to generate pellet 2 (P2). The resulting supernatant (S2) was centrifuged at 15000 x g for 10 minutes to generate pellet 3 (P3) followed by centrifugation of the S3 supernatant at 200000 x g for 70 min using a tabletop Beckman ultracentrifuge to generate the final S4 supernatant (SUP) and P4 pellet (P4). All pellets were resuspended in dPBS or 25 mM HEPES, pH 7.4 and proteins quantified by BCA assay (ThermoScientific, Rockford, IL).

Nucleic acid and Thioflavin S staining

Caput P2 and P4 and cauda P4 samples (each ~ 2-4 mg/ml) were diluted 1:4 in dPBS and 5 μl were spread on slides (Epredia Superfrost Plus, Portsmouth, NH) in a ~1cm x 1cm square and allowed to dry overnight. For SDS treatment, SDS was added to caput samples (1% final) for 15 min at RT and then samples were spread on slides to dry overnight. Cauda samples were spread on slides and dried overnight before exposure to 70% formic acid for 15 minutes at room temperature. All slides were then washed 3x in H_2O, 2 minutes each wash, before staining for nucleic acids and amyloid. For nucleic acids staining, slides were rehydrated with 25mM HEPES (Sytox Green) or dPBS (Hoechst, TOTO-3) for 2 minutes followed by incubation in 1μM Sytox Green (Invitrogen, Waltham, MA) in 25mM HEPES, 1μg/ml Hoechst 33342 in dPBS, or 10μM TOTO-3 (Molecular Probes, Eugene, OR) in dPBS for 15 minutes at room temperature in the dark. Mock-treated control slides were incubated in 25mM HEPES or dPBS. Slides were washed 3 x in 25mM HEPES or dPBS followed by 1x ddH_2O, 2 minutes per wash. Slides were mounted with Vectamount AQ (Vector Laboratories, Newark, CA) followed by imaging on a Zeiss Axiovert 200M microscope equipped with epifluorescence.

For Thioflavin S staining, slides were rehydrated with ddH_2O for 2 minutes before incubation in 0.1% Thioflavin S in ddH_20 (filtered) (Sigma, St. Louis, MO) in a Coplin jar for 2 hours at room temperature in the dark. Mock-treated control slides were incubated in ddH_2O without Thioflavin S. The slides were washed 3x in ddH_2O and 3x in 50% ethanol, 10 minutes per wash. Slides were washed 1x in ddH_2O followed by mounting with Vectamount AQ (Vector Laboratories, Newark, CA). In some experiments the ThS stained samples were also stained with propidium idodide. After the water wash, slides were equilibrated in dPBS by 3x 2 min washes and incubated with 20 μM propidium iodide for 15 min at RT in the dark. Slides were washed 3X in dPBS,1x ddH_20, 2 min each and mounted with Vectamount AQ. Images were captured on a Zeiss Axiovert 200M microscope equipped with epifluorescence.

Preparation of human DNAse1L3, DNase, and RNase treatment of epididymal amyloids

Human DNase1L3 was prepared as follows, aliquoted and stored at -80°C.[36] Briefly, approximately 100 grams of bacterial cells were suspended in 250 ml Lysis Buffer (20 mM HEPES at pH 7.4, 1 mM $CaCl_2$, and 300 mM NaCl). The cells were lysed using a hydraulic microfluidizer (Microfluidics M110EH, Microfluidics International Corp, Westwood, MA), and the resulting soluble cytosolic fraction was isolated via centrifugation at 19,500 rpm for 50 minutes using a JA20 rotor. The soluble fraction was then loaded onto a Ni^{2+}-NTA affinity column (Takara Ni-NTA), washed with wash buffer (20 mM HEPES pH 7.4, 1 mM $CaCl_2$, 300 mM NaCl, 30 mM Imidazole), and eluted with elution buffer (20 mM HEPES pH 7.4, 1 mM $CaCl_2$, 300 mM NaCl, 100 mM Imidazole). Before removing the polyhistidine-MBP (maltose binding protein) carrier protein with 1-2mg of TEV (Tobacco Etch Protease), 0.2mM PMSF was added to inhibit any bacterial serine proteases. In addition, 2mM Maltose was added to the protein sample to aid further purification. The TEV cleavage reaction was incubated at 4°C overnight. The sample was diluted with Buffer A (20 mM HEPES, pH 7.4, 1 mM $CaCl_2$) and loaded onto a SP Sepharose cation exchange column. The column was washed with Buffer A until the UV_{280} returned to baseline. The protein was then eluted with an isocratic gradient of 20% of Buffer B (20 mM HEPES, pH 7.4, 1 mM $CaCl_2$, 1 M NaCl), followed by a linear gradient 20-100% linear gradient of Buffer B over 150 ml. Subsequently, an SDS-PAGE gel was run to identify the appropriate elution fractions, which were then concentrated to 1 ml using an Amicon concentrator with a cutoff of 10 kDa, filtered through a 0.22 μm filter, and loaded onto an SD75 gel filtration column. Peak fractions from the gel filtration column were assessed for purity on an SDS-gel, concentrated to 1 mg/ml, snap frozen in liquid N_2, and stored at -80°C.

A fresh aliquot of DNAse1L3 was thawed on ice, diluted to 0.2 mg/ml with dPBS and used immediately. Thirty μgs of caput P2, caput P4 and cauda P4 amyloid fractions in 25 mM HEPES, pH 7.4 were incubated in a final volume of 40 μl containing 20 units SupeRase-In RNAse inhibitor (Invitrogen), and dPBS (start samples). Buffer treated samples (buffer) also included 1 mM $MgCl_2$, +EDTA samples included 1 mM $MgCl_2$ and

5 mM EDTA; and +DNase samples included 1 mM $MgCl_2$ and 5 μg/ml DNase1L3. All samples were incubated at 37°C for 1-4 hours. For RNase exposure, 30 μgs of caput and cauda amyloid fractions were incubated in a final volume of 40 μl containing dPBS and 1 μl (12.5 μg/ml final) DNase-free RNase in RNase buffer (10 mM Tris, pH 7.4, 5 mM $CaCl_2$, 50% glycerol) (Sigma) or RNase buffer alone at 37°C for 30 min. To determine the effect of nuclease treatment on amyloid content, 36 μl of the reactions were transferred to a 96 well plate and Thioflavin T (Sigma) added to 25 μM final or Sytox Orange (Invitrogen) added to 0.2 μM final and fluorescence measured after 5 min incubation at room temperature using a Tecan plate reader. ThT and Sytox Orange blank controls (all assay components except protein) were subtracted from the amyloid containing samples. Samples were done in duplicate or quadruplicate. The remaining 4 μl of the 40 μl total sample volume were spread on a slide (Epredia Superfrost Plus, Portsmouth, NH) dried overnight, and stained with ThS, as described above, or Sytox Orange as follows. Slides were washed 3x in 25 mM HEPES, 2 minutes per wash, incubated in 1 μM Sytox Orange (Invitrogen, Waltham, MA) for 15 minutes at room temperature in the dark, washed 3x in 25 mM HEPES, 1x in ddH_2O, 2 minutes per wash and then mounted with Vectamount AQ (Vector Laboratories, Newark, CA) followed by imaging on a Zeiss Axiovert 200M microscope equipped with epifluorescence.

Amylase treatment and wisteria floribunda agglutinin staining

One percent α-amylase (MP Biomedical) was prepared in dPBS and sterile filtered (0.22μm) before enzyme activation in a 37°C water bath for 30 minutes. Immediately after enzyme activation, caput and cauda P4 samples (15 μg) were incubated with α-amylase (0.1% final) in dPBS or dPBS alone (control) and reactions were carried out for 30 minutes - 4 hrs at 37°C. Five μls of each sample were spread on to slides in ~1cm x 1cm square and allowed to dry overnight. Slides were rehydrated with dPBS for 2 minutes before incubation in 1:500 wisteria floribunda agglutinin (Invitrogen, Waltham, MA) overnight at room temperature in the dark in a humidified chamber. The slides were washed 3x in dPBS and 1x in ddH_20, 2 minutes per wash. Slides were mounted with Vectamount AQ (Vector Laboratories, Newark, CA) followed by imaging on a Zeiss Axiovert 200M microscope equipped with epifluorescence.

To quantify changes in amyloid, amylase exposed samples were transferred to a 96 well plate, ThT added to 20 μM final and ThT fluorescence measured using a Tecan plate reader.

Alcian blue staining

CD-1 mouse paraffin-embedded epididymal tissue sections were deparaffinized through xylene (2 X 5 min each), rehydrated in ethanol (2 X 100%, 1 x 95% 2 min each) and water and stained with Alcian blue pH 2.5 (1% Alcian blue in 3% aqueous acetic acid, filtered) for 30 min in a Coplin jar. Slides were then put under running tap water for 2 min, rinsed in distilled water, dehydrated through ethanol (1x 95%, 2 X 100% 2 min each), cleared with xylene (1X 3 min) and mounted using Permount. Some tissue sections were counterstained with neutral red after Alcian blue staining. After the distilled water rinse, slides were incubated in 1% neutral red (in 0.1% acetic acid, filtered) for 1 min and then processed through ethanol and xylene as described for Alcian blue. For staining of isolated caput and cauda epididymal P4 amyloids, samples were spread on a slide and allowed to dry overnight. Slides were incubated in 1% Alcian blue, pH 2.5, pH 1.0 or pH 0.2 for 30 min, washed under running tap water (pH 2.5) or drained followed by a quick dip in distilled water (pH 1.0 and pH 0.2), dehydration through ethanol, xylene and mounting with Permount. One percent Alcian blue pH 1 was prepared in 0.1 N HCl while pH 0.2 was prepared in 10% sulfuric acid.

Collection of conditioned media

DC1 epididymal cells were grown until ~70-80% confluency. Cells were washed 2x with warmed HBSS, 2 minutes per wash. Cells were then incubated in IMDM media without phenol red and FBS but with all other additives at 37°C and 5% CO_2 for 16 hours. Conditioned media was collected and spun at 500 x g for 5 minutes to remove cells. The conditioned media was moved to new tubes and spun again to remove any remaining cells. Conditioned media was then concentrated in a 3 kDa Amicon-Ultra-15 filter to a volume of 500 μl. Protein concentrations were determined by BCA assay (ThermoScientific, Rockford, IL). Different amyloid fractions were then prepared as done with luminal fluid from the epididymis. One hundred and seventy-five μg of concentrated conditioned media was centrifuged at 5000 x g for 10 minutes to generate pellet 2 (P2). The resulting supernatant (S2) was centrifuged at 15000 x g for 10 minutes to generate pellet 3 (P3) followed by centrifugation of the S3 supernatant at 200000 x g for 70 min using a tabletop Beckman ultracentrifuge to generate the final S4 supernatant (SUP) and P4 pellet (P4). Five μls of the sample were spread on slides and allowed to dry overnight before staining.

Examination of nucleic acids by agarose gel electrophoresis

Twenty μg of supernatant (S4 supernatant, Figure 1B), P2, P4 and total (S1 supernatant, Figure 1B) from the caput and cauda epididymis and conditioned media from DC1 cells were diluted in dPBS to a final volume of 18 μl. Three μl of 6X loading buffer (Promega, Madison, WI) were added to each reaction and samples were run on a 1% agarose-TAE gel. Gels were stained with 2 μg/ml ethidium bromide (EtBr) for 20 minutes, washed in ddH_2O for 30 minutes and imaged on an Azure Biosystem C300.

Plasmid digestion assay

Five hundred ng of plasmid (pGEX-cs) were incubated with 0-5 μg/ml final DNase1 or DNase1L3 in 25 mM HEPES, pH 7.4, 0.5 mM $MgCL_2$ in a reaction volume of 18 μl for 10 minutes at 37°C. Samples were run on a 1% agarose-TAE gel followed by staining with 2 μg/ml EtBr for 20 minutes and washed in ddH_2O for 30 minutes. Gels were imaged on an Azure Biosystem C300.

Epididymal amyloid matrix degradation assay

Twenty μgs of caput and cauda P4 were incubated with 3.6 μl of DNase1 or DNase1L3 (0.5, 2, or 5 μg/ml final concentration) in DNase storage buffer (20 mM HEPES, pH 7.4, 1mM $CaCl_2$, 400 mM NaCl) and 4.5μl of 4X enzyme buffer (100 mM HEPES, pH 7.4, 2 mM $MgCl_2$). dPBS was used to bring the reactions to a final volume of 18 μl. Control reaction contained 3.6 μl of DNase storage buffer in place of DNase and 4.5μl of 4X enzyme buffer. Reactions were incubated for 1 hour at 37°. Reactions were run on a 1% agarose-TAE gel, stained with 2 μg/ml EtBr for 20 minutes and washed in ddH_2O for 30 minutes. Gels were imaged on an Azure Biosystem C300.

QUANTIFICATION AND STATISTICAL ANALYSIS

Statistical analyses were performed using ANOVA followed by multiple comparisons test or by t-test using GraphPad Prism software version 9.5.1. Details of the analyses including tests used, sample size (n), and significance values are included in the figure legends.